Chapter 2

Preparation and Characterization of modified forms of Palm Shell Powder

Outline:

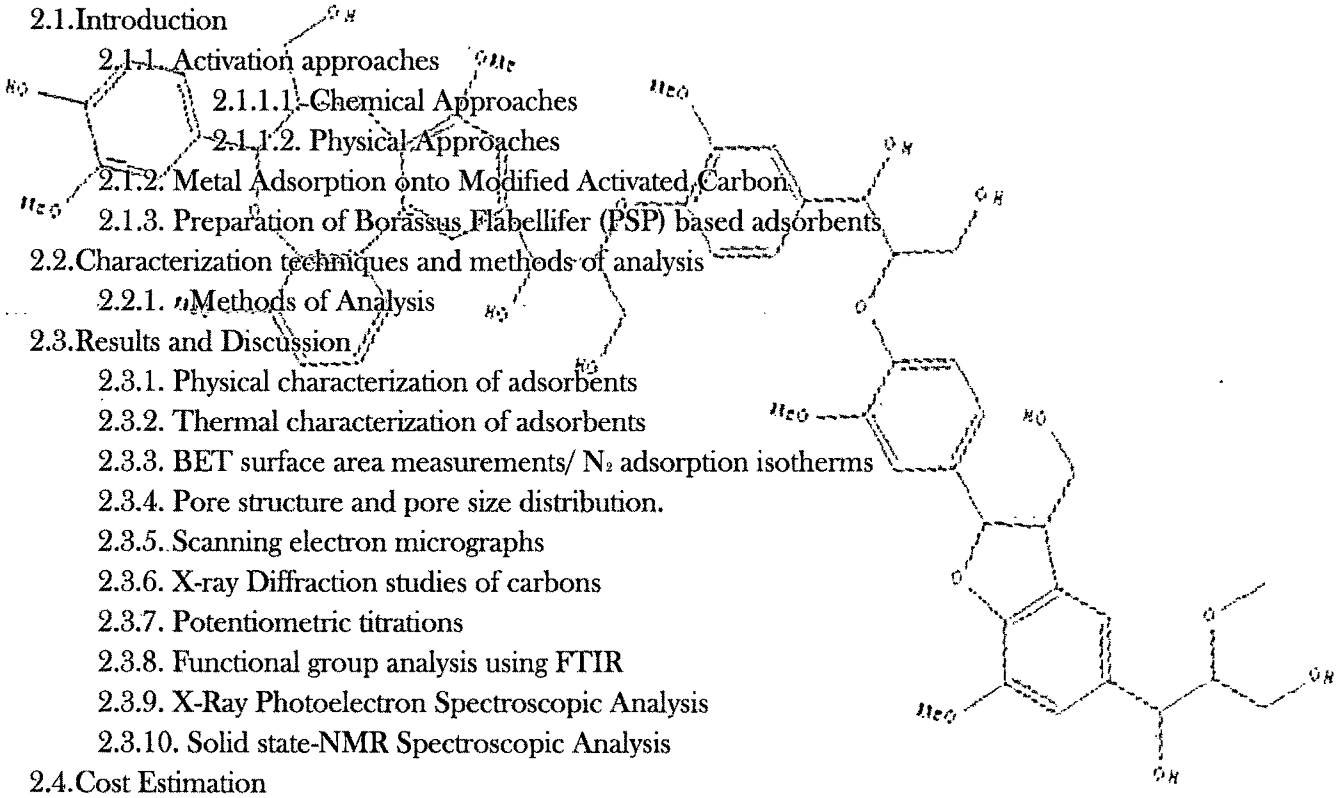

2.1. Introduction

Activated carbon has undoubtedly been the most popular and widely used adsorbent in wastewater treatment throughout the world. Activated carbon is well known as an efficient adsorbent because of its porosity and large surface area. It has thus been widely used in the sorption of gases and chemical species from aqueous solution. Precursors to activated carbons are either of botanical origin (e.g. wood, coconut shells and nut shells) or of degraded and coalified plant matter (e.g. peat, lignite and all ranks of coal). Agricultural by-products are considered as very important feedstock as they are renewable and low-cost materials [1, 2]. Agricultural materials particularly those containing cellulose shows potential sorption capacity for various pollutants. The basic components of the agricultural waste materials include hemicellulose, lignin, lipids, proteins, simple sugars, water, hydrocarbons, and starch, containing variety of functional groups.

Agricultural waste materials being economic and eco-friendly due to their unique chemical composition, availability in abundance, renewable nature and low cost are viable option for water and wastewater remediation. Agricultural waste is a rich source for activated carbon production due to its low ash content and reasonable hardness [3]. Therefore, conversion of agricultural wastes into low-cost adsorbents is a promising alternative to solve environmental problems and also to reduce the preparation costs. In the last several decades, various agricultural wastes have been explored as low-cost adsorbents [4]. Cost effective activated carbons can be prepared from a variety of agricultural wastes. Some of the most commonly used precursors have been given in Table 1.3 of chapter 1 which include nutshells, fruit stones, rice bran rice husk , coconut shell and oil palm shell due to ecological and economic significance [5-8].

Heavy metal adsorption onto activated carbons generally depends on their physical and chemical properties. Physical properties of carbons include their specific surface area, size, and porosity, whereas chemical properties are mainly determined by their surface functional groups, including carboxyls, carboxylic anhydrides, phenols, lactones, lactols, carbonyls, quinones, and quinone-like structures [9]. Activation of carbon surfaces by physicochemical methods has been studied so that metal removal can be enhanced to meet increasingly stringent environmental regulations [10, 11].

During the activation process, partial oxidation takes place and a pore structure develops. Generally activated carbons are produced by carbonizing the raw material prior to activation.

Carbonization is necessary to increase the carbon content and for the development of porous material. During carbonisation, pyrolytic decomposition of the precursor occurs [12] together with the concurrent elimination of many of the non-carbon elemental species (H, N, O and S). Low molecular weight volatiles are first released, followed by light aromatics and finally, hydrogen gas [13], the resultant product being a fixed carbonaceous char [14]. The pores formed during carbonisation are filled with tarry pyrolysis residues and require activation in order to develop the internal surface of the char [15]. During the activation process, the spaces between the elementary crystallites are cleared by removal of less organized loosely bound carbonaceous material. The resulting channels through the graphitic regions, the spaces between the elementary crystallites, together with fissures within and parallel to the graphite planes constitute the porous structure, with a large internal surface area [16]. Two types of activation, thermal/physical or chemical activation, impart a porous structure within a starting material of relatively low surface area [17].

Carbonization temperature affects the shapes of pores in the carbon. High temperature char samples have higher micro-pore volume [18, 19]. To prepare mesoporous carbons activation to high burn off degrees, physical and chemical activation [20-25], catalytic activation in the presence of transition metals [26, 27] and template carbonization [28-31] have been used.

2.1.1. Activation Approaches.

Carbon surface can be activated to develop desirable physicochemical properties by adequate choice of activation procedures (Figure 2.1). It is even possible to prepare carbons with designated proportions of micro-, meso-, and macropores.

2.1.1.1. ***Chemical Approaches.*** Chemical activation employs a catalyst, metallic chlorides or acid impregnation into the raw material to influence the pyrolysis such that tar formation and volatilization are kept to minimum [32]. The most widely used chemical activants are $ZnCl_2$, H_3PO_4, H_2SO_4, KOH, K_2S, oxidizing agents and KCNS [33]. The feedstock is impregnated with the catalyst, often as a near saturated solution, dried and then carbonised and activated in a single action although two separate temperatures are often used. Post activation treatment is required to remove residual catalyst which may be reclaimed for subsequent reuse. Chemical activation is performed at temperatures of between 400-800°C and used industrially for wood-based carbons.

The pore size distribution of the final product is largely a function of the degree of initial impregnation [34].

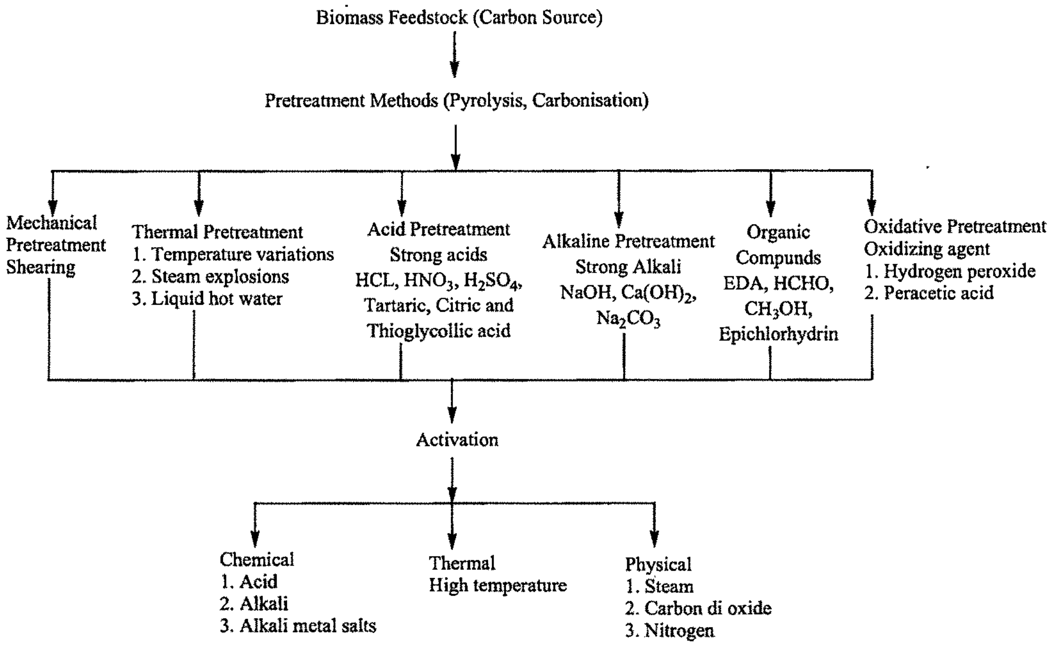

Figure 2.1. Methods of activation

Treatment by acids, bases, or oxidizing agents produces favorable chemical and physical properties for different applications (e.g. separation and catalysis). Gas phase oxidation mainly increases the content of hydroxyl and carbonyl surface groups, while liquid phase oxidation enhances especially that of carboxylic groups [35].

The modification by inorganic acids mainly changes the surface chemistry of the carbons and sometimes alters their specific surface area and porosity. For example, treatment of carbon by phosphoric acid can cause a high surface area and high degree of porosity [36-38]. Both strongly and weakly acidic oxygen functional groups can be introduced by acid modification [39].

Oxidation of activated carbons by H_2O_2 increases hydroxide groups in the oxidized products when the solution pH is not controlled. However, when the solution pH is fixed at 2.5 or 11.5, the hydroxide groups decrease while other oxygen groups (e.g., carbonyl and carboxyl) increase [40].

HNO_3 treatment increases the quantity of acidic surface functional groups [41]. Various surface oxygen groups and structures containing N-O bonds (nitro groups and nitrate complexes) are developed [42]. Mazet et al. showed a significant increase in the surface area, while Gomez-Serrano et al. observed a slight variation [43].

Carbons with well-developed meso- and microporous structure have been produced by $ZnCl_2$ incorporation. KOH activation successfully increased active carbon surface area and pore volume [44]. Ammonium salts, borates, calcium oxide, ferric and ferrous compounds, manganese dioxide, nickel salts, hydrochloric acid, nitric acid and sulfuric acid have also been used for activation. Polymers and chelating agents have been selected to modify activated carbons. The density of positive surface charges on the carbons can be increased after they are grafted by cationic polymers [45, 46]. The quantity of surface functional groups is also changed [47].

2.1.1.2. ***Physical Approaches.*** Carbons can be treated physically for improvement of their properties for different applications. It is reported that heat treatment in an inert atmosphere can selectively remove some functional groups. Partial gasification refers to the direct reaction between the carbonised char and an activant in its gaseous or vapour state. As in chemical activation, the principle objective is the removal of tarry amorphous carbon from the interstitial layers of the structure in order to develop the porosity and make accessible the internal surface area. Porosity develops with increased burn-off of disorganised carbon [48]. Steam, carbon dioxide and air are the most common activants, the kinetics and mechanisms of these reactions being well known for many years [49-52].

Surface carboxylic acid groups of carbons disappear after treatment in H2 at 723 K [39]. De la Puente et al. observed the removal of carboxylic acid groups at the temperature of 400-623 K [53]. The elimination of stable ether groups was found at temperatures above 823 K. At higher temperatures, the concentrations of carboxylic acid groups decrease and, subsequently, ketone and quinone groups disappear [54]. With a further increase in the temperature, elimination of both the ether groups and the aliphatic structures occurs [55].

Menendez et al. modified an activated carbon by a microwave device under nitrogen flow [56]. Most acidic oxygen groups are removed from the carbon surface, resulting in a significant increase in the carbon pH. The basic differences between physical and chemical activation is the number of stages required for activation and the activation temperature. Chemical activation occurs in one step while physical activation employs two steps, carbonization and activation.

Physical activation temperatures (800–1000 ^{0}C) are higher than those of chemical activation (200–800 ^{0}C).

According to Steenberg's classification [57], acidic and basic activated carbons exist: Depending on the extent of the oxidizing reaction, two forms of activated carbons can be produced [58, 59].

(a) Carbon activated at 200–400 ^{0}C, called L carbons, generally develop acidic surface oxides and lower solution pH values. They adsorb bases, are hydrophilic, and exhibit a negative zeta potential.

(b) The carbons activated at 800–1000 ^{0}C, termed H carbons, develop basic surface oxides are hydrophobic and raise solution pH. They adsorb acids and exhibit a positive zeta potential. However, cooling H carbons in contact with air changes the zeta potential to a negative value due to the formation of acidic surface oxides.

The acidic groups on activated carbons adsorb metal ions [60]. The L carbons are stronger solid acids than the H carbons and more efficiently adsorb metal ions. Garten *et al.* have suggested carboxyl, phenolic hydroxyl, carbonyl (quinone type), carboxylic acid, anhydrides, lactone, and cyclic peroxide as the predominant surface functional groups of L-carbons [61].

Surface area may not be a primary factor for adsorption on activated carbon. High surface area does not necessarily mean high adsorption capacity [62] due to the following factors:

(a) Only the wetted surface adsorbs ions. The total surface area is seldom wetted.

(b) Sometimes the material to be adsorbed is too large to enter the smallest pores where the bulk of the surface area may exist.

(c) Surface area, pore volume and surface chemistry are not usually correlated with species adsorbed.

The adsorption of metal ions on carbon is more complex than uptake of organic compounds because ionic charges affect removal kinetics from solution. Adsorption capacity depends on activated carbon properties, adsorbate chemical properties, temperature, pH, ionic strength, etc. Many activated carbons are available commercially but few are selective for heavy metals. As they are expensive improved and tailor-made materials are sought. Substitutes should be easily available, cheap and, above all, be readily regenerated, providing quantitative recovery. Industrial or agricultural by-products can be converted into activated carbons or low cost adsorbents.

The raw ligno-cellulosic biosorbents are modified by various chemical methods either to increase the metal adsorption capacity or to prevent leaching [63-66]. However, typically almost all carbonizations are conducted at high temperatures (300–800 °C) [67].

To the best of our knowledge very few reports are available in the literature on the combined treatment of agrowaste with combined acid (H_2SO_4) and chemical activation (persulfate or hydrogen peroxide) at temperatures as low as 140°C [68]. As the effect of this treatment on palm shell (*Borassus Flabellifer*), which is available throughout coastal Asia has not been reported, it was decided to explore the potential of palm shell as raw material to prepare various adsorbents. Thus, the possibility of preparing adsorbents from palm shell powder (PSP) using concentrated sulfuric acid for charring and charring in the presence of oxidizing chemicals like $K_2S_2O_8$ have been explored. Adsorbent was also prepared by thermal activation to 900°C for comparison.

2.1.2. **Metal Adsorption onto Modified Activated Carbon.**

Heavy metal adsorption onto activated carbons is due to a series of adsorption reactions between the metal ions and the organic functional groups in the carbons. The adsorptive behaviors maybe significantly altered after the surfaces of carbons are modified [69-72].

Heat-treated activated carbons can significantly improve the adsorption capacity [42]. Anodic oxidation of carbon results in enhancement of both uptake capacity and kinetics for Cr^{6+}. Air oxidation can cause an improvement in copper adsorption [70]. In the copper adsorption onto a sulfuric acid-modified carbon, it was observed that the concentration of acidic surface oxides on the carbon surfaces increased and cation exchange reactions occurred [71]. On the other hand, the copper adsorption onto a carbon treated in an ammonia atmosphere is due to the formation of surface complexes with the nitrogen- and oxygen-containing functional groups [72].

Since modification of adsorbent surface might change the properties of adsorbent, it is recommended that for any work on chemically modified plant wastes, characterization studies involving surface area, pore size, porosity, pH_{ZPC}, etc. are also carried out. Spectroscopic analyses involving Fourier transform infrared (FTIR), Nuclear Magnetic Resonance Spectroscopy(NMR), X-ray photoelectron spectroscopy (XPS) were also done to have a better understanding on the mechanism of metal adsorption on modified plant wastes.

Outer shell of palm fruit (Borassus Flabellifer) is a cheap and abundant agricultural by-product in tropical countries. Hence objective of this work was:

i) To study the feasibility of the use of palm shell powder as a precursor for the preparation of different adsorbents by charring using H_2SO_4 (APSP) at 140^0C, steam treatment of APSP (SAPSP), persulfate treatment of APSP (PAPSP), activation to higher temperatures of APSP (3AAC, 6AAC, 7AAC and 9AAC) and formaldehyde treatment of PSP, APSP, SAPSP and PAPSP (MPSP, MAPSP, MSAPSP and MPAPSP)

ii) To characterize all the prepared materials as well as palm shell powder for their physicochemical characteristics and compare the surface area, porosity and surface chemistry of the prepared materials.

2.1.3. Preparation of Borassus Flabellifer (PSP) based adsorbents

The shells of palm fruit (Borassus Flabellifer) were collected from coastal Andhra Pradesh, India, and were cut into small pieces. The pieces were extensively washed with running tap water for 30 to 40 minutes to remove dirt and other particulate matter followed by double distilled water. The pieces were dried in an oven at 70^0C, ground in a laboratory blender and sorted using standard test sieves. The sample used was of particle size passing 40 micron sieve and is henceforth termed as palm shell powder (PSP).

The PSP was modified by using different techniques (Scheme 2.2). PSP was treated with conc. H_2SO_4 in a ratio of 1:1.5 weight/volume with continuous stirring. The charred substance was then heated in an air oven at 140^0C for 24h. The sample was then extensively washed with a solution of 2% $NaHCO_3$ until the effervescence ceased, and further kept soaked in 2% $NaHCO_3$ overnight. After washing with distilled water 2-3 times, the sample was then kept in an air oven for 4 hrs at 105^0C. The prepared acid treated palm shell powder is termed as APSP.

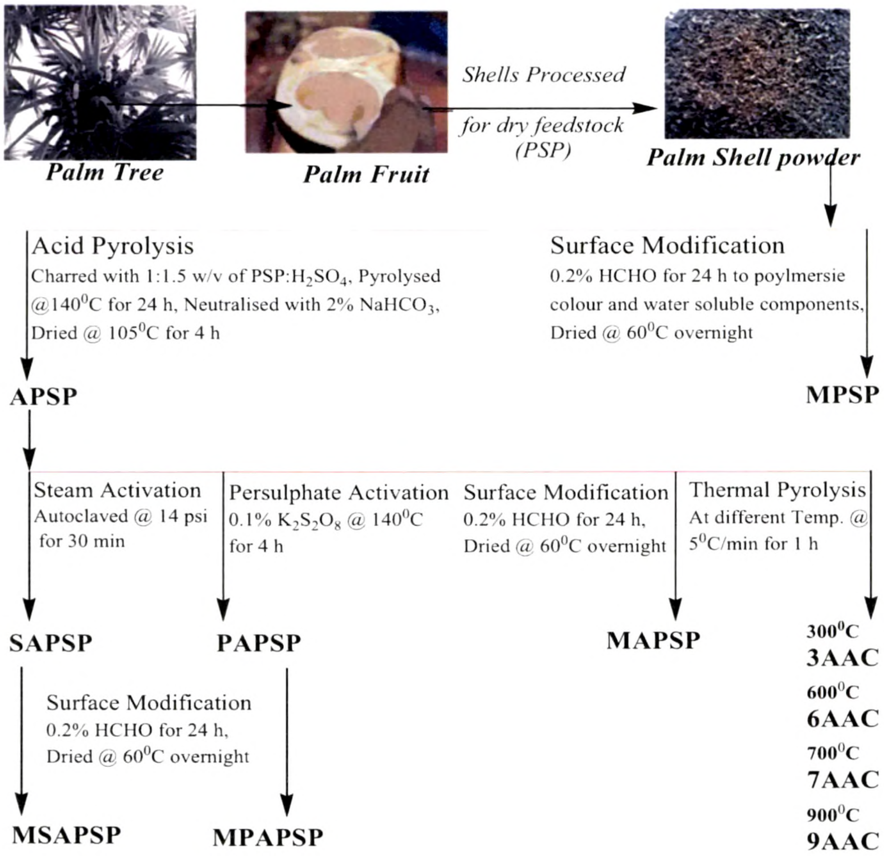

Scheme 2. Different methods of modification of palm shell powder

APSP was modified by different methods- i) APSP was treated with steam in an electric autoclave for 30 minutes at 14psi pressure and the product obtained was termed as SAPSP. ii) PAPSP was obtained by treating APSP with conc. H_2SO_4 in the ratio of 1: 1.5 wt/volume in presence of 0.1% $K_2S_2O_8$ and was kept in an air oven for 4 hrs at 140^0C. Subsequently it was washed extensively with 2% $NaHCO_3$ until effervescence ceased and left overnight, soaked in 2% $NaHCO_3$. Finally it was washed 2-3 times with distilled water and then again dried in an air oven at 105^0C for 4hrs.

Modification of PSP, APSP, SAPSP and PAPSP with formaldehyde was done in order to polymerize and immobilize the color and water soluble substances. One gram each of PSP, APSP, SAPSP and PAPSP were soaked in 100 mL of 0.2% formaldehyde solution for 24 h. The resulting MPSP, MAPSP, MSAPSP and MPAPSP were then filtered, washed with 300 mL of distilled water several times, and dried overnight in an oven at 60°C.

To see the effect of temperature on surface area of APSP, thermal activation was done at four different temperatures 300^0C (3AAC), 600^0C (6AAC), 700^0C (7AAC), 900^0C (9AAC). The heating was carried out with a programmable muffle furnace at a rate of $5^0C/min$ until the desired temperatures were reached and then kept at that temperature for one hour. The samples 3AAC, 6AAC, 7AAC and 9AAC were then washed with 2% $NaHCO_3$ until effervescence ceased, and were left soaked in 2% $NaHCO_3$ overnight. Finally they were washed 2-3 times with distilled water and then again dried in an air oven at 105^0C for 4hrs.

2.2. Characterization techniques and methods of analysis

The surface chemistry of adsorbents has been indicated to have a significant effect on the uptake of various adsorbate molecules. The changes in the surface chemistry of the adsorbents under study were followed by potentiometric titrations and data analysis, Solid state ^{13}C NMR, X-ray photoelectron spectroscopy, X-ray powder diffraction (XRD), Braunett-Emett-Teller (BET), Scanning Electron Microscopy (SEM), Thermogravimetric analysis (TGA) and Fourier transform infrared spectroscopy. The specific surface area of the adsorbent, pore volume and pore size can be measured by the BET method (N_2 adsorption–desorption). The surface images of samples were obtained using SEM. DTA–TGA was employed to analyze the population of surface functional groups on the basis of thermal stability. Fourier transform infrared (FTIR) analysis was applied to determine the surface functional groups. XPS helps in interpreting the surface features of the adsorbents.

2.2.1. Methods of Analysis

Physical properties (bulk density, moisture content, solubility in water and acid) and chemical properties (pH, ion exchange capacity) of the prepared adsorbents were investigated. **Bulk density** measurements were done using a previously weighed 100mL graduated cylinder and filling it up to 50 mL mark with the adsorbent under study. The cylinder with the carbon was weighed accurately. The apparent density was calculated by dividing the difference in weight by 50. **Moisture content** was found out by heating a known weight of the sample in an air oven maintained at 105 ± 5^0C for about 4 hr. Heating, cooling and weighing were repeated at 30 min time interval till the difference between two consecutive weighings was less than 5 mg. **Solubility in water and acid** was determined by taking ten gram of adsorbent under study into a one litre beaker and boiling with 300 mL distilled water and 0.25 N HCl respectively followed by digestion for around 30 min. The material was washed thoroughly with distilled water and washings were collected along with the filtrate. The filtrate was concentrated on a water bath, cooled and made up to 100 mL in a volumetric flask. Exactly 50 mL of the concentrate was transferred to a china dish, evaporated to almost dryness on a water bath and finally dried in an electric oven maintained at105 ± 5^0C, cooled and weighed. The weight of the residue represents the matter soluble in water and acid. The **pH** was measured by heating a suspension of ten gram adsorbent in 300 mL distilled water to boiling with constant stirring. The solution was then digested for around 30 minutes. The material was filtered, cooled and pH of the solution was measured. For measuring the **ion exchange capacity**, 0.5 g of adsorbent under study was added to 100 mL solution of 0.25M sodium sulphate in a stoppered conical flask and kept for shaking in a temperature controlled shaking bath for 5 hours. The contents were filtered and the filtrate was titrated against 0.1N NaOH using phenolphthalein indicator. The ion exchange capacity of the adsorbent in meq/g was calculated from the following equation.

$$\textbf{Ion exchange capacity}\left(\frac{\textbf{meq}}{\textbf{g}}\right)=\frac{\textbf{aW}}{V}$$

Where, a = Normality of NaOH

V = Volume of NaOH

W = Weight of the adsorbent in g

Iodine Value was calculated by means of adsorption of iodine from aqueous solution which can be used to compare adsorbent surface areas and is a relative indicator of porosity [73]. A sample of 0.2 g of adsorbent under study was equilibrated with iodine/iodide solution and the iodine residual concentration was determined by titrating with sodium thiosulphate solution.

Iodine Value = (Blank-Burette reading for sample) x Conversion factor; mg/g.

$$\textbf{Conversion factor}=\frac{\textbf{Mol. Wt. of Iodine (127) x 40}}{\textbf{Wt. of Carbon x Blank Reading}}$$

Blank Reading: Burette reading for iodine concentration without adding the carbon sample. Burette reading for sample: Burette reading for iodine remaining unadsorbed in solution after adding the carbon sample.

The iodine number is a relative indicator of porosity in a carbonaceous material and may be used as an approximation of surface area for some types of carbons [73]. Correlation between the Braunett-Emett-Teller surface area and the iodine number is established and well documented [8, 74, 75]. As iodine number gives an indication on micro-porosity (pores less than

1 nm in diameter), higher iodine numbers reflect better development of the micro-porous structure and higher adsorption abilities for low-molar-mass solutes [74, 76, 77]. All the experiments were carried out in triplicate and the average results are provided.

Potentiometric experiments were carried out using an adsorbent mass of 0.1 g suspended in 50 mL of 0.01 M KNO_3 solution, and the suspension was left for 24 h in contact with the electrolyte. The suspensions were acidified to pH 3.0 using 0.1 M HNO_3 and then titrated to pH 11 using 0.1 M NaOH. All experiments were conducted in triplicate in a glass vessel with a lid as part of a Spectralab AT-38C automatic potentiometric titrator. The temperature was recorded with a temperature sensor; the error of the temperature probe was 0.1 ^{0}C. The pH electrode was three-point calibrated with buffers (pH 4, 7, and 10) before each experiment, and the slope did not deviate more than 1 % from the Nernst value. The titrator unit was programmed with a step volume dose mode for the titration, which adds 0.001 mL of titration solution according to the pH changes.

Data Analysis. The titration data were analyzed using the linear programming method (LPM) approach or so called pK_a spectrum method as proposed by Brassard [78]. Proton dissociation from the surface ligands can be described by the following equation:

$$\mathrm{HL^0} \leftrightarrow \mathrm{H^+} + \mathrm{L^-}$$

Where L^- is the proton binding site on the surface and H^+ is the protons in solution. The concentration of protonated and deprotonated surface sites can be quantified with the corresponding mass action equation.

$$K_\mathrm{a} = \frac{[\mathrm{H^+}][\mathrm{L^-}]}{[\mathrm{HL^0}]}$$

Where K_a is the acidity constant.

The titration data are expressed in the form of charge excess versus $-\log[H^+]$. Where charge excess (b $= C_b - C_a + [H^+] - K_w/[H^+]$) for the known concentration of acid (C_a) and base (C_b) was calculated for the jth addition of acid and base, the charge balance expression can be written as

$$b_j = \sum_{i=1}^{n}[\mathrm{L}_i^-] + S = \sum_{i=1}^{n}\left(\frac{\mathrm{L}_{Ti}K_{ai}}{K_{ai} + [\mathrm{H^+}]_j}\right) + S$$

S is a constant term analogous to the acid neutralizing capacity (ANC) as in Brassard. This equation could be solved by setting the number of sites (n) and varyingL_{Ti} and K_i. This is essentially what FITEQL does, where n is increased until the fit is good enough. To avoid selecting n and to prevent convergence problems caused by the correlation of L_{Ti} *and* K_i, it is preferable to fix the pK_a values as a grid from a minimum to a maximum value at fixed step sizes. The ligand concentration associated with each pK_a is assigned a positive value where zero is a possible result; the result is the so called pK_a spectrum. For the data here the minimum and maximum pK_a values corresponds to the measured minimum and maximum pH, respectively, and the step size is fixed at 0.2. The pH range was selected because Smith (http://info.wlu.ca/wwwchem/faculty/Smith/Research/research.shtml) demonstrates the errors for acid base titrations outside this range are very large. The pK_a spectrum approach is used here to determine the best fit of K_{ai}/L_{Ti} pairs, with pK_a values fixed as a grid from 4 to 10 at fixed step sizes (0.2). Once the pK_a values are selected, the matrix version of eq 3 is set up as $Ax = b$. The entry α_{ij} in the $m \times n$ matrix A for n proposed sites and m additions of titrant is

$$\alpha_{ij} = \frac{K_{ai}}{K_{ai} + [H^{+}]j}$$

The matrices used to solve the linear programming problem were set up as in Brassard and solved using Matlab linear programming routine.

The thermal behavior of the adsorbents was evaluated by using thermo-gravimetric analyzer (TG-DTA 32, SEIKO Thermal Analysis System SS 5100), under air at a heating rate of 10°C min^{-1}.

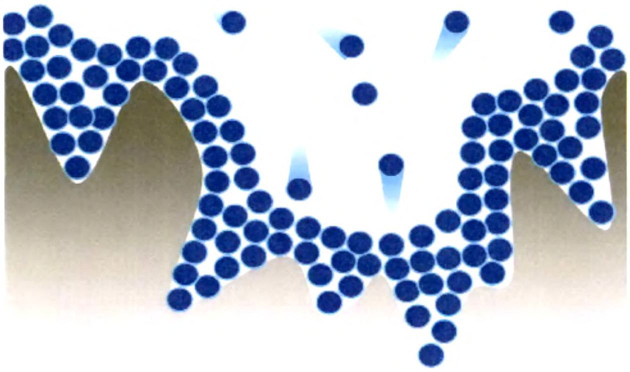

The porous structure of the adsorbents was determined by nitrogen adsorption at 77.37K (Surface Area Analyser Micromeritics, ASAP 2020 V3.03H). Nitrogen adsorption isotherm was measured over a relative pressure (P/P0) range from approximately 0.03 to 1. The specific surface areas were determined from the isotherms using the Brunauer–Emmett–Teller equation. BET isotherm is an extension of the Langmuir theory, which explains monolayer molecular adsorption capacity, to multilayer adsorption with the following hypotheses: (a) gas molecules physically adsorb on a solid in layers infinitely; (b) there is no interaction between each adsorption layer; and (c) the Langmuir theory can be applied to each layer. The resulting **BET equation** is expressed by:

$$\frac{1}{v\left[\left(\frac{P_0}{P}\right)-1\right]}=\frac{c-1}{v_m c}\left(\frac{P}{P_0}\right)+\frac{1}{v_m c}$$

P and P_0 are the equilibrium and the saturation pressure of adsorbates at the temperature of adsorption, v is the adsorbed gas quantity (for example, in volume units), and v_m is the monolayer adsorbed gas quantity. c is the BET constant, which is expressed by:

$$c = exp\left(\frac{E_1 - E_L}{RT}\right)$$

E_1 is the heat of adsorption for the first layer, and E_L is that for the second and higher layers and is equal to the heat of liquefaction.

Nitrogen adsorption results can be plotted using $1/v[(P_0/P) - 1]$ on the y-axis and relative pressure P/P_0 on the x-axis. This plot is called a **BET plot.** The linear relationship of this equation is maintained only in the range of $0.05 < P/P_0 < 0.35$. The value of the slope A and the y-intercept I of the line are used to calculate the monolayer adsorbed gas quantity v_m and the BET constant c. The following equations can be used:

$$v_m = \frac{1}{A+I}$$

$$c = 1 + \frac{A}{I}$$

BET method is widely used in surface science for the calculation of surface areas of solids by physical adsorption of gas molecules. A total surface area S_{total} and a specific surface area S are evaluated by the following equations:

$$S_{BET,total} = \frac{(v_m N_s)}{V}$$

$$S_{BET} = \frac{S_{total}}{a}$$

N: Avogadro's number, v_m: molar volume of the adsorbate gas in terms of volume, s: adsorption cross section of the adsorbing species, V: molar volume of adsorbate gas, a: mass of adsorbent (g) [79].

The cross-sectional area of a nitrogen molecule was assumed to be 0.162 nm^2. The t-plot and DR plot methods were applied to calculate the pore volume and the BJH method was used for pore size distribution determination [7, 80].

Multi-layer formation is modeled mathematically to calculate a layer "thickness, t" as a function of increasing relative pressure (P/P_o). The resulting t-curve is compared with the experimental isotherm in the form of a t-plot. That is, experimental quantity adsorbed is plotted versus statistical thickness for each experimental P/P_o value. The linear range lies between monolayer and capillary condensation. The slope of the t-plot (V/t) is equal to the "external area", i.e. the area of those pores that are not micropores. Mesopores, macropores and the outside surface are able to form a multilayer, whereas micropores, which have already been filled, cannot contribute further to the adsorption process. Harkins and Jura equation was employed to interpret the t-plot micropore area and external surface area.

$$t = \left[\frac{13.99}{\left(0.034 - log\left(\frac{P}{P_0}\right)\right)}\right]^{0.5}$$

BJH method was used for describing pore volume and pore size using Halsey equation with Faas correction. Condensation occurs in pores that already have some multilayers on the walls. Severely underestimates size of small to medium mesopores and acceptable for broad size distributions of medium to large mesopores.

$$t = 3.54 \times \left[\frac{-5}{\left(ln\left(\frac{P}{P_0}\right)\right)}\right]^{0.33}$$

Dubinin-Radushkevich (DR) analysis has been devoted to elucidating the micropore structures of various solids regardless of insufficient understanding of the basis of the DR equation. In particular, activated carbon whose micropore structure cannot be determined by other characterization techniques has been analyzed by the DR equation.

$$W = W_0 e^{\left[-\left(\frac{A}{E}\right)^n\right]}$$

$n=2$, $E=\beta E_0$, $A=RT\ln(P_0/P)$

W and W_0 are the amount of adsorption at the relative pressure $P/P0$ and the micropore volume, respectively. A is the adsorption potential. β and E_0 are the affinity coefficient and characteristic adsorption energy, respectively. Plot of ln W versus A^2 relationship which linearizes the isotherm based on micropore filling principle. Best fit is extrapolated to A^2 to find the micropore volume. Useful to find micropore volume when chosen analysis conditions do not aloe complete filling.

The surface morphology and topographic analysis of the adsorbent samples was examined by Scanning Electron Microscope (JEOL, Model JSM-5610LV). Samples were mounted onto metal holders using a conducting substrate.

Powder-XRD of the ingredients was taken by holding the samples in place on quartz plate for exposure to CuKα radiation of wavelength 1.5406 Å. The sample was analyzed at room temperature over a range of $10\text{-}70^0$ 2θ with sampling intervals of 0.02^0 2θ and scanning rate of 6^0 /min.

FT-IR-The functional groups in the materials under study were characterized by infrared spectroscopy (Fourier Transform Infra Red spectra were collected by a Perkin Elmer RX1 model within the wave number range of $400\text{-}4000\text{cm}^{-1}$. Specimens of samples were first mixed with KBr and then ground in an agate mortar at an appropriate ratio of 1/100 for the preparation of the pellets. Resulting mixture was pressed at 10 tons for 5 min. sixteen scans and 8cm^{-1} resolution were applied in recording spectra. The background obtained from the scan of pure KBr was automatically subtracted from the sample spectra.

XPS is a surface technique which will provide an estimate of the chemical composition of the few uppermost layers of the material. The materials under study were analyzed by XPS to determine the chemical states of the surface functional groups. The surface of the samples was analyzed using a KRATOS AXIS 165 X-ray Photoelectron spectrometer equipped with dual aluminum–magnesium anodes using Mg Kα radiation. The X-ray power supply was run at 15 kV and 5 mA. The pressure of the analysis chamber during the scan was 10^9 Torr. Peak fitting and presentation output are produced by an integrated VISION control and information system. The deconvolution process of C 1s spectra as well as the elemental composition evaluation may result in an error of up to 5%. All spectra are presented charge balanced and energy referenced to C 1s at 284.6 eV [81]. Chemical states of O, N and C species were determined from the charge corrected hi-resolution scans. The atomic concentrations were estimated based on comparisons of integrated peak intensities normalized by the atomic sensitivity factors.

Solid state ^{13}C NMR describes the detailed components present in the adsorbents. The study of the structure and properties of carbon materials by nuclear magnetic resonance (NMR) has been a subject of increasing interest in recent years. ^{13}C nuclei belonging to aromatic carbons resonate at a frequency range readily separated from the aliphatic ones, providing important information about the structure of these materials. Applications in the study of coals, cokes, charcoals, chars, polymeric carbons, amorphous carbons and new carbon forms have been reported [82-90]. The ^{13}C-NMR experiments were performed with a Bruker Avance (300 MHz) spectrometer. The chemical shifts δ, expressed in parts per million [ppm], were referenced relative to the signal of tetramethylsilane (TMS) at $\delta c = 0$ ppm.

2.3. Result and Discussion

2.3.1. Physical characterization of adsorbents.

The series of adsorbents namely APSP, SAPSP, PAPSP, MAPSP, MSAPSP, MPAPSP, 3AAC, 6AAC, 7AAC and 9AAC prepared from PSP by different routes and different activating agents were characterized for various characteristics like bulk density, solubility in water, solubility in acid, ash content, moisture content and ion exchange capacity and are tabulated in Table 2.1.

Table 2.1. Physical characterization of sorbents

Sample	Bulk density	Moisture Content	pH	Solubility in H_2O	Solubility in acid	Ion exchange capacity	Ash content
	gm/cm^3	%		%	%	meq/gm	%
PS	0.351	8.37	6.00	3.44	4.04	0.004	0.897
APSP	0.550	2.60	8.05	12.33	15.61	0.125	6.653
SAPSP	0.576	14.58	7.75	53.40	51.20	0.110	6.893
PAPSP	0.626	16.34	8.00	25.30	27.70	0.071	6.783
MPSP	0.362	9.34	7.10	2.50	3.91	0.500	1.098
MAPSP	0.553	15.32	6.80	10.00	13.06	0.250	5.470
MSAPSP	0.578	19.14	6.41	36.50	38.10	0.124	5.230
MPAPSP	0.551	17.62	6.32	6.00	8.10	0.125	6.980
3AAC	0.648	11.56	7.60	3.50	4.20	0.014	1.409
6AAC	0.549	9.32	6.99	3.50	4.71	0.250	4.678
7AAC	0.448	9.08	6.95	0.01	0.04	0.167	9.532
9AAC	0.539	15.90	6.90	0.50	0.92	0.167	10.989

It can be observed from the table that bulk density of activated carbons in each case is higher than PSP. Moisture content was in the range of 2.6–19.1%. The moisture content detected was due to the contact of moisture from atmosphere after activation. Solubility in water and acid is negligible for PSP, MPSP, 3AAC, 6AAC, 7AAC and 9AAC. All the adsorbents prepared have pH in the range (6.0-8.0) which is appropriate for water treatment purpose. APSP, SAPSP, PAPSP, 3AAC have a pH of ~7.5–8.0 while the others have a neutral to near neutral pH of 6.0-7.1. pH values of the adsorbents under study are lower than reported pH values of commercial activated carbons. Ion exchange capacity is significantly increased and was found to be the highest for MPSP (0.5) followed by MAPSP and 6AAC (0.25), 7AAC and 9AAC (0.167), APSP (0.125) and SAPSP (0.110). The other modified forms had comparatively low ion exchange capacity.

Adsorbents that can remove a high percentage of iodine normally have a high surface area and also largely a micro- and mesoporous structure [91]. It can be seen from the Figure 2.2 that on modification with formaldehyde the iodine value was higher (312.41 mg/g) as compared to PSP (146.82 mg/g) but was slightly lower to that of APSP (342.47 mg/g). Temperature variation from 300°C to 900°C during thermal activation of APSP resulted in an increase in iodine value from 436.82 to 990.44 mg/g which is comparable with reported values.

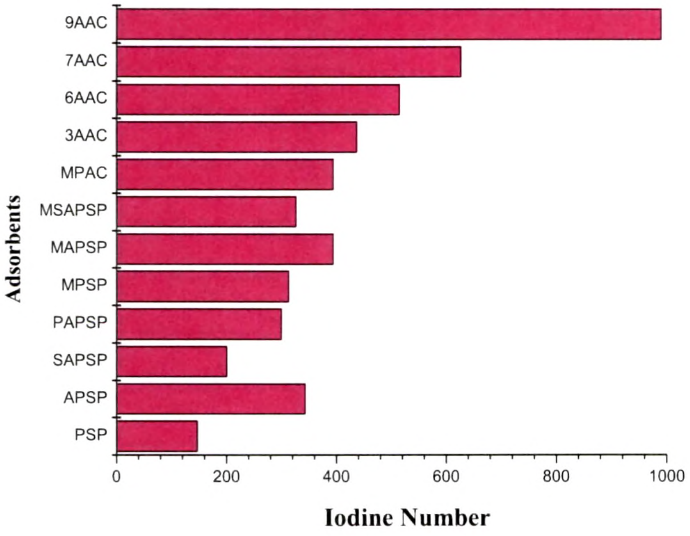

Figure 2.2. Iodine Number of the adsorbents under study

2.3.2. Thermal characterization of adsorbents.

Thermal analysis curves (DTG, DTA and TGA) are shown (Figure 2.3). The weight loss during thermo-gravimetric decomposition of the adsorbents can be divided into different stages and tabulated in Table 2.2.

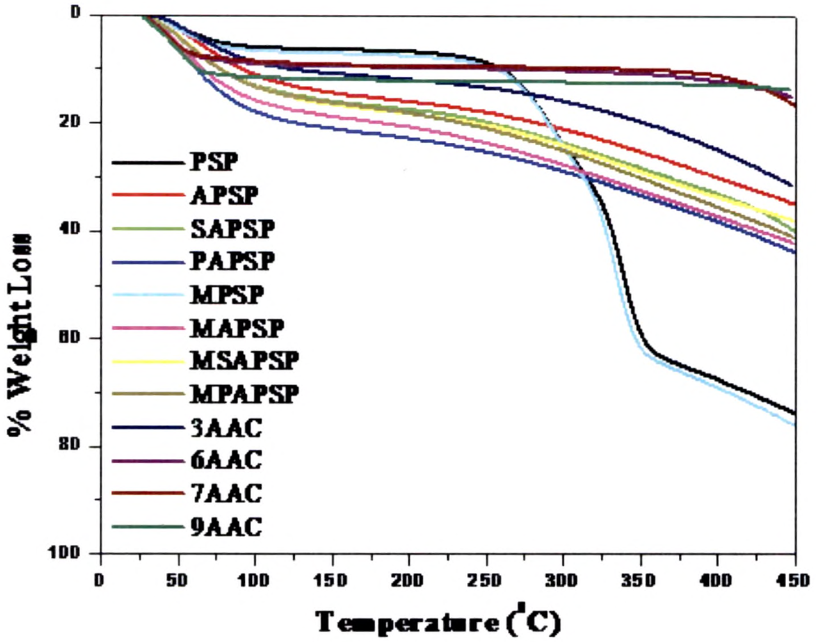

Figure 2.3. Thermal Analysis of Activated Carbons

Table 2.2. Thermal analysis

Sample	Weight loss (%)							
	1st stage	Temperature range (°C)	2nd Stage	Temperature range (°C)	3rd Stage	Temperature range (°C)	4th Stage	Temperature range (°C)
PSP	5.610	26.1 – 99.9	89.21	207.3 – 493.7	-	-	1.91	493.7 – 858.3
APSP	10.480	30.5 – 99.9	36.00	99.9- 478.0	8.20	478.0 - 746.4	31.6	746.4 - 829.2
SAPSP	13.900	28.3 – 124.5	-	-	38.59	124.5 – 750.9	33.54	750.9 – 858.3
PAPSP	14.570	30.5 – 129.0	61.71	129.0 – 578.7	1.92	578.7 – 748.7	9.60	748.7 – 860.5
MPSP	6.059	30.5 – 205.1	90.50	205.1 – 495.9	-	-	2.10	495.9 – 858.3
MAPSP	16.596	30.6 – 135.7	54.60	135.7 – 585.4	-	-	19.90	585.4 – 860.6
MSAPSP	11.040	26.1 – 102.2	-	-	40.08	102.2 – 717.4	33.29	717.4 – 858.3
MPAPSP	15.199	30.5 – 144.6	62.50	144.6 – 558.5	-	-	10.10	708.4 – 858.3
3AAC	12.745	28.3 – 135.7	83.60	135.7 – 486.9	-	-	1.30	486.9 – 858.3
6AAC	7.147	30.6 – 102.1	2.10	102.1- 305.7	86.10	305.7 – 560.8	-	-
7AAC	4.560	30.5 – 95.4	33.50	95.4 – 372.8	80.00	372.8 – 547.3	-	-
9AAC	4.326	32.8 – 84.3	4.25	84.3 – 406.4	80.40	406.4 – 623.4	-	-

The TGA curves of the adsorbents showed a first stage weight loss of about 4-16% in the region below 145°C corresponding to the loss of water molecules. The second stage
(145°C< T<600°C), which corresponds to the primary carbonization, is seen as a large weight loss for the adsorbents, suggesting the elimination of volatile matters and tars. Above 600°C, SAPSP, PAPSP, MAPSP, MPAPSP and 3AAC showed very little weight loss indicating their decomposition to a structure with higher stability while APSP and MAPSP showed a higher weight loss, indicating that more surface functional groups are created on APSP and MAPSP [92]. The TGA curves indicate that thermal stability is greater for 9AAC. Gergova [93] and Krisztina [94] have also reported three stages in the carbonization process and the formation of basic structure at 800-900^{0}C in ligno-cellulosic materials.

2.3.3. BET surface area measurements/ N_2 adsorption isotherms.

Adsorption isotherms of nitrogen for the adsorbents are shown in Figure 2.4. N_2 uptake was found to be very less in PSP, APSP, SAPSP, PAPSP, MPSP, MAPSP, MSAPSP, MPAPSP and 3AAC. The shapes of the isotherms are different as a result of different porosities. The porosities seem to be same for MPSP, MAAC, MSAPSP and 3AAC and similar for APSP, PSP and PAPSP. Predominant adsorption finishes at a very low relative pressure and the amount of nitrogen adsorbed decreased for 3AAC, MAPSP, MPSP, PSP indicating that pore cavities are micro-porous/ blocked. The nitrogen adsorption isotherms of 9AAC, 7AAC and 6AAC show increase in amount of nitrogen adsorbed with relative pressure which reflect a certain amount of meso-pore volume. It is observed that the carbons 6AAC and 7AAC exhibit type II isotherms, indicating an indefinite multi-layer formation after completion of the monolayer and is found in adsorbents with a wide distribution of pore sizes. Near to the first point of inflexion a monolayer is completed, following which adsorption occurs in successive layers, while 9AAC exhibits type IV adsorption curve with a hysteresis loop (in the relative pressure range of 0.8-1), which is associated with capillary condensation in meso-pores.

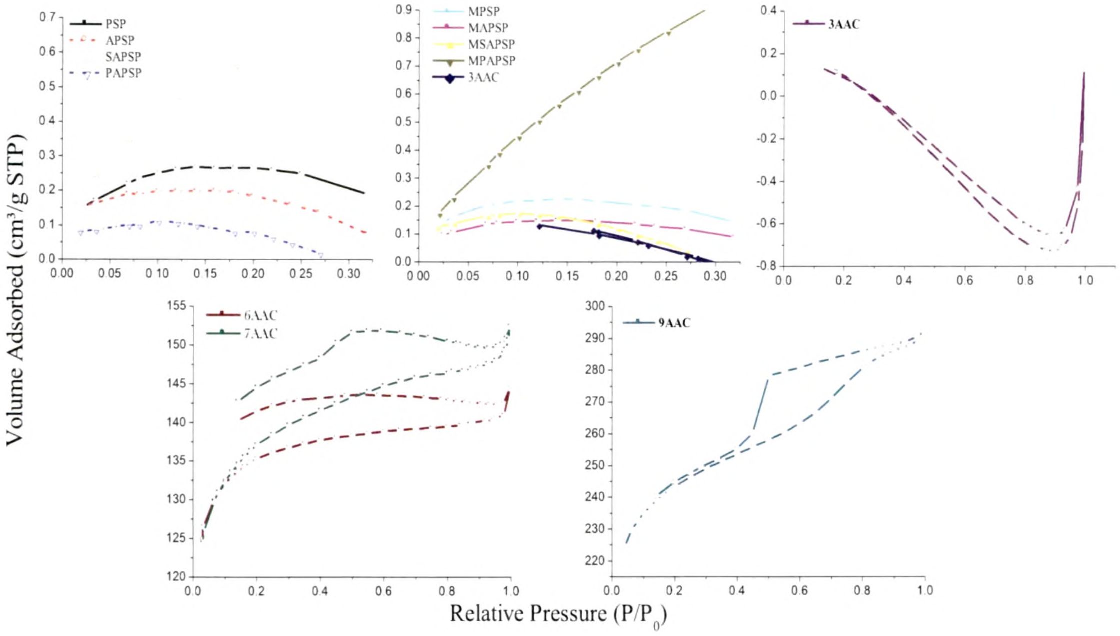

Figure 2.4. Adsorption isotherms of nitrogen for the adsorbents

The hysteresis loops are different in 6AAC, 7AAC suggesting the presence of pores with different shapes. The nitrogen adsorption isotherm of 9AAC shows a tremendous increase in N_2 uptake compared to 6AAC and 7AAC. The adsorption was found to be higher at low relative pressure for 6AAC, 7AAC and 9AAC suggesting the presence of relatively larger number of micro-pores. Type III isotherm is obtained for 3AAC which occurs when affinity between adsorbent and adsorbate is less than adsorbate-adsorbate interactions. BET isotherm is not applicable for calculation of surface area in such adsorbents.

PSP, APSP, SAPSP, PAPSP, MPSP, MAPSP, MSAPSP, MPAPSP show type I isotherm according to BET classification indicating monolayer adsorption and are typical of micro-porous samples and hence not amenable to BET analysis [95].

Table 2.3. Surface Area Analysis

Adsorbent	Single point SA	BET SA	Langmuir SA	BJH Pore SA	BJH Pore Volume	BET Av. Pore dia.
Unit	m^2/g	m^2/g	m^2/g	m^2/g	cm^3/g	Å
PSP	0.562	0.673	0.965	-	0.004	237.984
APSP	0.217	0.297	0.408	-	0.003	422.652
SAPSP	2.134	2.419	3.894	-	0.005	81.244
PAPSP	0.056	0.090	0.115	-	0.022	9829.990
MPSP	0.424	0.504	0.714	-	0.004	301.040
MAPSP	0.260	0.314	0.442	-	0.0016	201.730
MSAPSP	2.810	3.405	6.344	-	0.0055	64.240
MPAPSP	0.121	0.176	0.225	-	0.001	243.823
3AAC	0.254	0.113	0.132	-	0.001	-
6AAC	470.793	469.586	596.925	50.481	0.218	18.569
7AAC	477.179	476.194	606.997	79.780	0.230	19.349
9AAC	846.334	834.874	1083.357	162.848	0.447	21.436

BET surface area measured for different activated carbons is presented in Table 2.3. The carbons APSP, SAPSP, PAPSP, MAPSP, MSAPSP and MPAPSP do not show high BET surface area but adsorption property as seen by iodine value is higher. They may contain a number of narrow micropores inaccessible (within reasonable time) to N_2 at 77 K [96]. The iodine number is considered as a simple method to evaluate the surface area of activated carbons associated with pores with d>1nm. The carbons prepared at higher carbonization temperatures (6AAC, 7AAC and 9AAC) have significantly increased pore volume (~0.218, 0.23 and 0.447 cm^3/g) and BET surface area (~469.586, 476.194 and 834.874 m^2/g); with supportive evidence from iodine values. BET surface area is higher than BJH surface area, which agrees well with observations made by Gregg and Sough [97]. Complete decomposition of PSP could not be achieved even at 700^0C. Thus the low surface area of 3AAC, 6AAC and 7AAC are due to the presence of non decomposed or partially decomposed products in the pores of the carbon. On heating to 900^0C the decomposition of these products was also complete and pores were liberated and surface area increased to $846m^2/g$. BET surface area is highest for 9AAC forming mainly micro-pores. A comparison has been made for the surface area of different activated carbons and presented in

Table 2.4. It is evident that the surface area of 9AAC is comparable to that of other activated carbons prepared from agro-wastes reported in literature.

Table 2.4. Comparison of surface area of adsorbents

Raw material	Carbonisation conditions ^{0}C/hr	Activation conditions ^{0}C/hr	Chemical Treatment	BET Surface area m^2/g	Ref.
Grape seeds	800/1 hr (15^{0}C/min)	800/1 hr	Steam activation, one step pyrolysis/ activation	497	[18]
Nut shells	800/1 hr (15^{0}C/min)	800/1 hr	Steam activation, one step pyrolysis/ activation	743	[18]
Pistachio-nut shells	500/ 2hr (10^{0}C/min)	900/ 30min (10^{0}C/min)	Physical activation, CO_2	778	[30]
Macadamia nut shells	1 hr	500^{0}C	Chemical activation with both $ZnCl_2$ and KOH	1718	[31]
Peanut hulls	500/2 hr	700-900^{0}C	Physical activation, two step	80.8-97.1 420	[29]
Almond shells	800/1 hr (15^{0}C/min)	800/1 hr	Steam activation, One step pyrolysis/ activation	998	[18]
Oat hulls	500^{0}C/ (1.5sec residence)	800/ 30 min	Steam activation	625	[7]
Cotton stalk	400-700^{0}C with 7^{0}C/min	-	-	3.14 37.28	[5]
Oak	700-800^{0}C	-	Residence time 1-2 hr	985	[28]
Corn hulls	700-800^{0}C	-	Residence time 1-2 hr	1010	[28]
Corn Stover	700-800^{0}C	-	Residence time 1-2 hr	660	[28]
Olive seed	800/ 1hr	800-900^{0}C	Residence time 1-2 hr, Chemical activation, KOH	1550	[105]
Rice straw	700-1000/ 1hr (10^{0}C/min)	900^{0}C	Chemical activation, KOH, Two step method	2410	[106]
Rice husk	-	600^{0}C/ 3hr	Chemical activation, one step, $ZnCl_2$/ CO_2	480	[107]
Pecan shell	-	-	Chemical activation, (H_3PO_4),	724	[108]
Cassava peel	650/ 3hr	750^{0}C	Chemical activation, KOH	1183	[109]
9AAC	105^{0}C/ 1hr	900^{0}C	Carbonization using H_2SO_4	834	This study

2.3.4. Pore structure and pore size distribution.

The extent of the microporosity and the development of the pore structure under different conditions used were evaluated by identifying the micro- and mesopore volumes and pore size distributions presented in Figure 2.5.

Micropore volumes were analyzed by DR and t-plots as shown in Table 2.5. The *t*-plot [29] estimates the pore volume by assuming that layers build up on the wall of the pores until the pore is completely filled. The DR method [98] describes the adsorption according to the mechanism of volume filling. It can be seen from Table 2.5 that the *t*-plot slightly underestimates the micropore volume showing values lower than those from DR. This feature is probably due to the high values of the surface area. Remy and Poncelet [99] suggested that the DR equation overestimated $W_{0,DR}$, with respect to $W_{0,t}$, when a solid presents an high surface area. The micropore volumes determined from the DR plot (Figure 2.6) increase with increase in temperature of APSP.

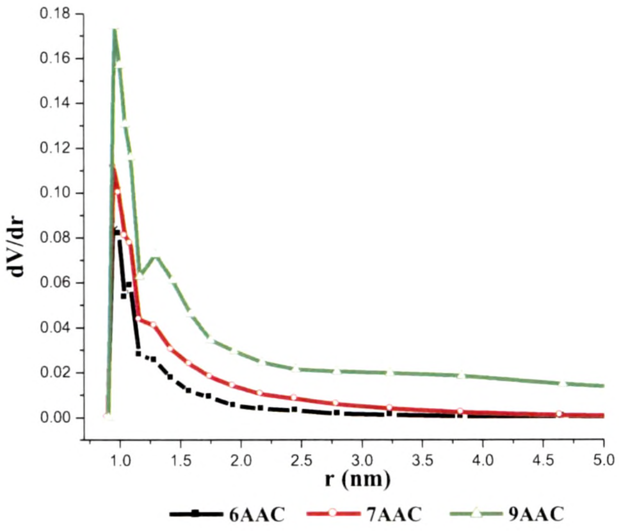

Figure 2.5. Pore size distribution graph

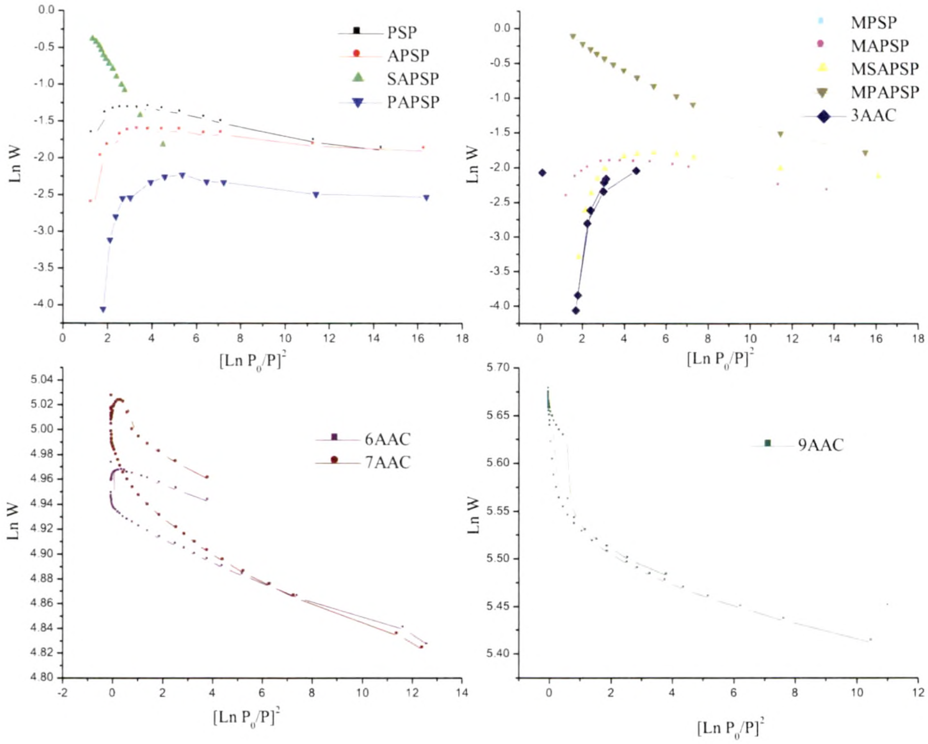

Figure 2.6. DR Plot for the adsorbents

For 6AAC, 7AAC and 9AAC, DR plots exhibited a brief linear range and then deviated upward indicating formation of multilayer and capillary condensation in the mesopores. Furthermore the mesopores (2-50 nm) increased with increase in temperature of activation i.e. increasing the extent of burn off (6AAC, 7AAC and 9AAC) as a consequence of enhanced pore formation and pore widening effect. Micro-pore volumes for 6AAC, 7AAC and 9AAC are in the range of 0.18-0.30 which is comparable to those reported in literature [7]. Thus increase of carbonization temperature resulted in creation of micropore structure and widening of micro-pores to mesopores and an increase in the total pore volume of carbons as seen in Table 2.5. Similar observations were made by D. Adinata et al. and Ismadji and Bhatia [100-102].

Table 2.5. Constants from DR Plot for the adsorbents

Adsorbent	E	E_0	W_0	Micropore volume (t-plot)	Mesopore volume
Unit	KJmol^{-1}	KJmol^{-1}	cm^3/g	cm^3/g	cm^3/g
PSP	4.227	12.432	0.00052	-	-
APSP	6.456	18.988	0.00034	-	-
SAPSP	1.456	4.2823	0.00195	-	-
PAPSP	6.153	18.097	0.00019	-	-
MPSP	4.567	13.432	0.00042	-	-
MAPSP	4.654	13.689	0.00028	-	-
MSAPSP	5.489	16.144	0.00032	-	-
MPAPSP	2.872	8.198	0.00146	-	-
3AAC	0.906	2.665	0.0000005	-	-
6AAC	11.070	32.559	0.21387	0.179	0.034
7AAC	9.027	26.55	0.22088	0.168	0.062
9AAC	7.925	23.309	0.39874	0.295	0.152

gas volumes were multiplied by 0.001547 to get liquid volumes

The pores of the carbons 6AAC, 7AAC and 9AAC are mostly located in the range of micropores with a peak at 1.2 nm. It is seen from Tables 2.3 and 2.5 that BET surface area as well as micropore volume were highest for 9AAC suggesting that micropores make the largest contribution to the surface area. At high carbonization temperatures more ordered structure is likely to be developed in the carbon that leads to a lower rate of gasification in the interior of the particles [103]. Thus activated carbon high in microporosity is produced. PSP, APSP, SAPSP, PAPSP showed small BET surface area and small pore volume suggesting the entry of the gas molecules was partially restricted.

The value of E_0 provides a first indication for the presence or absence of microporosity in carbons. Typical micropores correspond to E_0>18–20 kJ mol^{-1} (APSP, PAPSP, 6AAC, 7AAC and 9AAC), whereas values below 14–15 kJ mol^{-1} reflect either variable degrees of surface heterogeneity, or the presence of super micropores (1.5–2.5 nm) (PSP, SAPSP, formaldehyde treated adsorbents, 3AAC) [104].

2.3.5. Scanning electron micrographs.

The micrographs in Figure 2.7 show the surface morphologies of PSP and the prepared adsorbents. The activated and modified adsorbents are having large particle size which is developed like a coral shell. A channel of tubes passing through can be observed. Cross section of some particles has been taken showing distorted pores. Porosity can be seen but not homogeneous, and some pores are broken also which may not support adsorption, in SAPSP and MSAPSP. The pores are superficial and bulk of the sample does not seem to have any porosity, resulting in less surface area. In 6AAC, 7AAC and 9AAC defined surface porosity is seen to develop with temperature. Bulk porosity distributed in an even manner can be observed in some of the cross sections suggesting possible higher adsorption capacity as supported by iodine number and BET surface area parameters.

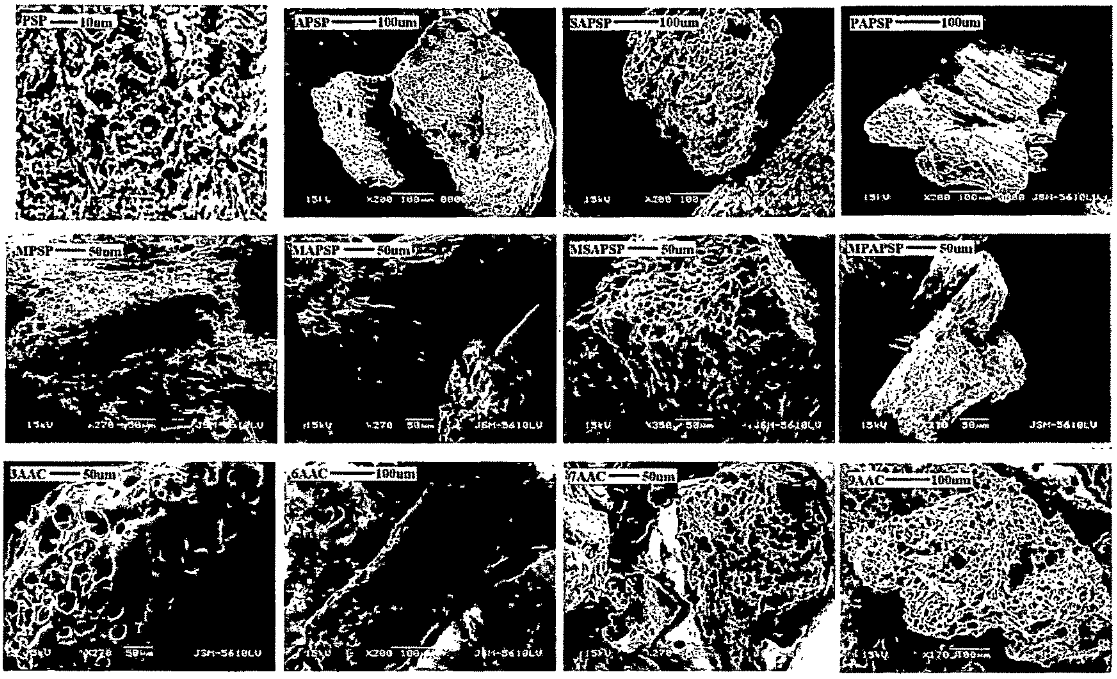

Figure 2.7. Scanning Electron Micrographs

2.3.6. X-ray Diffraction studies of carbons.

The X-ray diffraction patterns of PSP and the other adsorbents under study are presented in Figure 2.8 with the major peaks and their respective 2θ values tabulated in Table 2.6. XRD shows no characteristic peaks after activation at higher temperature. (6AAC, &7AAC and 9 AAC) suggesting turbostratic structure of disordered carbon materials. There is a broad peak at

2θ value of 25^0 for all the materials under study. Sharp non-labelled peaks in PSP, APSP, SAPSP, PAPSP, and MPSP show miscellaneous inorganic components. Peak spacings of PSP and APSP at 0.430 and 0.281nm are assigned to nkl 200 and 004 crystallographic planes of completely ordered regions of cellulose respectively, if a monoclinic unit cell is assumed with C as the fiber axis [110]. It is observed that in MSAPSP, MPAPSP the strong peaks are progressively losing intensity and becoming broader indicating a gradual decrease in cellulose crystallinity. A complete loss of crystal structure in cellulose is indicated by disappearance of 0.160 nm signals and shift of ~0.420 nm signal to higher angles in 3AAC, 6AAC, 7AAC and 9AAC. Similar observations were reported by Marko Kleber during activation at different temperatures [111].

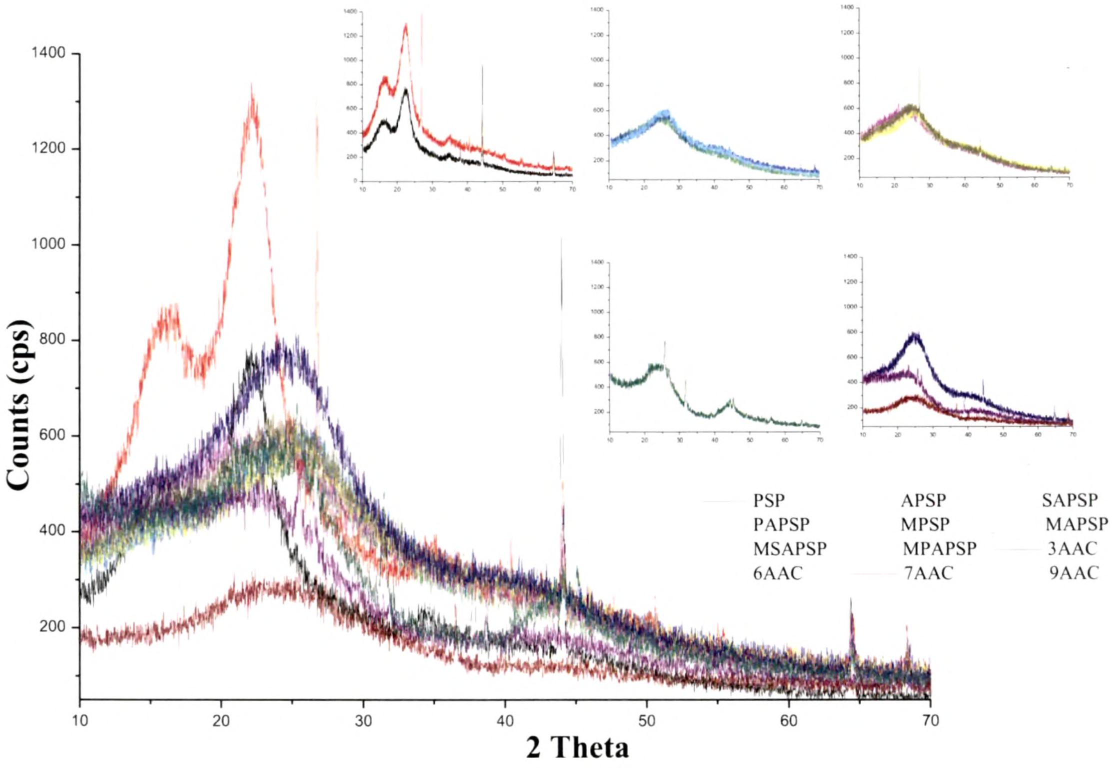

Figure 2.8. X-Ray Diffraction analysis

Peak spacings at ~0.60, ~0.53nm in MPSP and PSP can be assigned to101, 110 crystallographic planes of cellulose. Increased intensity of the 101 and 100 planes at 0.220nm in MPSP indicates lateral growth of graphene planes. Broadening of XRD signal with increasing temperature at ~0.37nm (23^0) in 7AAC suggests the dominance of small aromatic units arranged in random order which may be attributed to the (002) reflection of a graphitic-type lattice. A weak reflection centered around 43° corresponds to a superposition of the (100) and (101) reflections of a graphitic-type carbon structure, indicating a limited degree of graphitization in this material [112]. Narrowing of peak ~0.4nm with increasing temperature indicates developing atomic order in 9AAC and is attributed to the formation of turbostatic crystallites, i.e. progressive stacking of graphene sheets [113, 114].

Table 2.6. XRD analysis

Sr. No.	Sample	Peak
1.	PSP	10^0, 23^0, 27^0 and 34^0
2	APSP	9.22^0, 20.55^0, 20.0865^0, 26.827^0 and 31.8145^0
3	SAPSP	10^0, 27^0 and 32^0
4	PAPSP	10^0 and 27^0
5	MPSP	17^0, 23^0 and 25^0
6	MAPSP	25^0
7	MSAPSP	25^0
8	MPAPSP	25^0
9	3AAC	
10	6AAC	-
11	7AAC	-
12	9AAC	-

NOTE: From the above studies it is seen that no observable advantageous difference in properties were seen for MAPSP, MSAPSP, MPAPSP as compared to MPSP and similarly in 3AAC, 6AAC and 7AAC. Based on the characteristics of the prepared materials we decided to restrict further detailed characterization only for PSP, APSP, SAPSP, PAPSP, 9AAC and MPSP and their use as adsorbents in our further studies.

2.3.7. Potentiometric titrations.

The surface acidity of the carbons studied was estimated using potentiometric titration experiments. The pK_a distribution curves (Figure 2.9) show differences in surface groups of the adsorbents under study.

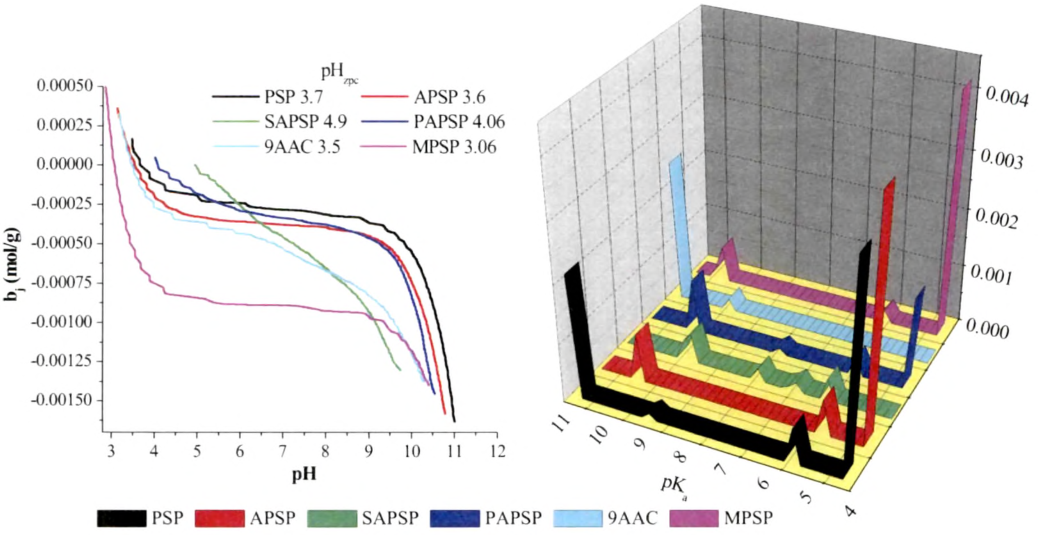

Figure 2.9. Potentiometric titrations and data analysis

Carboxyl groups are considered to have pK_a values <8 and those groups with pK_a >8 are classified as phenols and quinines [115]. However presence of adjacent electron-withdrawing groups increase acidity and decrease basicity. Thus the presence of greater number of acidic groups in APSP and MPSP could be due to the treatment favoring the fixation of carboxyl groups adjacent to acid enhancing groups [116]. In the case of PAPSP and SAPSP very little proton uptake is noticed. Treatment of APSP with steam results in a heterogeneous surface with pK_a at about 5.6, 6.4, 7.4, 9.2 and 9.5. This broad distribution indicates the existence of a wide spectrum of organic acidic groups covering the range of pK_a associated with both carboxylic and phenolic groups. On heating APSP to 900°C (9AAC) the concentration of surface groups at pK_a 11 slightly increased. Phenolic compounds were created in PSP, SAPSP and 9AAC. The number of acidic groups with pK_a 4 increased in MPSP and APSP while in 9AAC the number of acidic groups decreased significantly. Weaker acidic groups of pK_a in the range 5-6 are present in all the adsorbents under study (Table 2.7). Figure 2.9 shows the proton isotherms and zero point of charge (pH_{ZPC}) values of the adsorbents under study. The pH_{ZPC} values increase in the order

MPSP (3.06) > 9AAC (3.5) > APSP (3.6) > PSP (3.7) > PAPSP (4.06) > SAPSP (4.9). MPSP, 9AAC, APSP and PSP were found to exhibit low pH_{ZPC} values. The surface is positively charged at pH values below the pH_{ZPC}, since the oxygen-containing groups are undissociated and the adsorbent will remove anionic species from solution under these conditions. On the other hand, at solution pH values greater than the pH_{ZPC}, the adsorbent surface becomes more negative due to dissociation of weakly acidic oxygen-containing groups. Thus, the adsorbent surface has the possibility to attract and exchange cations in solution.

Table 2.7. Three-site model from pK_a analysis for titration data of adsorbents under study by linear programming

Ligand Class	1	2	3	4	Total Conc. (mol/g)
Range of pK_a	4.0– 5.0	5.0-7.0	7.0 - 9.0	9.0 – 11.0	
Functional Group	Carboxyl	Lactone	Amine	Hydroxyl/ Phenol	
Adsorbents	pK_a (L_T mol/g)				
PSP	4.0 (0.0036)	5.4 (0.0006)	9.0 (0.0001)	11.0 (0.021)	0.00633
APSP	4.0 (0.0041)	5.2 (0.0006)	-	10.0 (0.001)	0.00480
SAPSP	-	6.2 (0.0002)	7.5 (0.0001)	9.3 (0.0004)	0.00060
PAPSP	4.0 (0.0016)	5.4 (0.0003)	7.4 (0.0001)	9.8 (0.0009)	0.00290
9AAC	-	-	-	10.2 (0.0013)	0.00130
MPSP	4.0 (0.0042)	5.6 (0.0002)	-	10.3 (0.0004)	0.00480

2.3.8. Functional group analysis using FTIR.

The possible modifications in the functional groups of palm shell upon charring and activation were studied by infrared spectroscopy (Table 2.8 and Figure 2.10).

The presence of absorption bands characteristic of $-CH_3$ or $-CH_2$ symmetric stretching vibrations in the spectra of all the adsorbents suggests the existence of some aliphatic species on all the adsorbents under study. For PSP, APSP, PAPSP and SAPSP the bands in the frequency range 1723 to 1732 cm^{-1} indicate the presence of carboxylic acid groups as shown in Table 2.8. On charring with sulphuric acid (APSP) a new band at 1770 cm^{-1} appears which is characteristic of carbonyl moieties in carboxylic anhydrides [117-125]. The band at ~1348 to 1373 cm^{-1} for the adsorbents under study corresponds to vibrations in alkanes and alkyl groups, whereas the band near 1589-1597cm^{-1} is attributed to aromatic ring stretching coupled to highly conjugated carbonyl groups. The presence of bands at 1101 to 1180cm^{-1} in 3AAC, PSP and MPSP can be attributed to stretching frequency of the bonds in ester, ether and the phenol groups. 1348-

1373cm^{-1} is the characteristic peak of carbohydrates seen in PSP, APSP, SAPSP, PAPSP and MPSP. After formaldehyde treatment there seems to be a slight change in morphology probably due to the reaction of hydroxyl groups of cellulose with formaldehyde which is indicated by the absence of bands in the frequency range 1723-1732 cm^{-1} [125].

Table 2.8. FTIR Analysis

PSP	**MPSP**	**APSP**	**SAPSP**	**PAPSP**	**9AAC**	**Assignment**
3361	3389	3584	3489	3597	-	-N-H, -O-H stretching
-	-	-	-	-	2100	$-CH_3$, $-CH_2$ symmetric stretch
2959, 2895	2891	3036, 2876	2887	3078, 2887	3009, 2875	Free CO_2
1732	1727	1720	1723	1723	-	-C=O stretch for acids or aldehyde
1648	1666	-	-	-	-	-C=O stretch of Enolic group, nonconjugated lignin, amide/ -C=C- Aromatic stretch
1597	1597	1596	1597	1597	1589	-C=O stretch cellulose/ C=C Aromatic stretch (skeletal vibration)/ N-H bending of amide
1454	1477	1484	1488	1484	1484	$-CH_2-$ stretching
1430	1436	1438	1430	1433	1436	-C=C- Aromatic stretching
1373	1354	1344	1350	1356	1348	-C-H stretch/ N-H bending
1250	1238	1229	1229	1256	1208	-C-O bending of carboxylic acids/ phenolic O-H stretch/ N-H bending
1101	1161	-	-	-	-	-O-H stretch (2^0 Alcohol), -C-O-C- stretching
1049	1051	1044	1052	1035	-	-C-H stretch, -C-O stretch (1^0 Alcohol)
893	897	-	-	-	-	Anomeric C-H bending of cellulose
809	837	842	-	800	846	-C-H out of plane bending

The bands at 1079.82, 835.91 cm^{-1} are characteristic of carbohydrate units [126]. The bands for 3AAC at 1592cm^{-1}, MPSP at 1512 and 1387cm^{-1}, MSAPSP at 1578 and 1375cm^{-1}and APSP at 1378cm^{-1} suggests that lignin present in palm shell is still not completely depolymerised. The presence of bands at 1725cm^{-1} in the case of PAPSP, and at 1734cm^{-1} in PSP & MPSP is indicative of –C=O stretching of aromatic esters, aldehydes, ketones and acetyl derivatives.

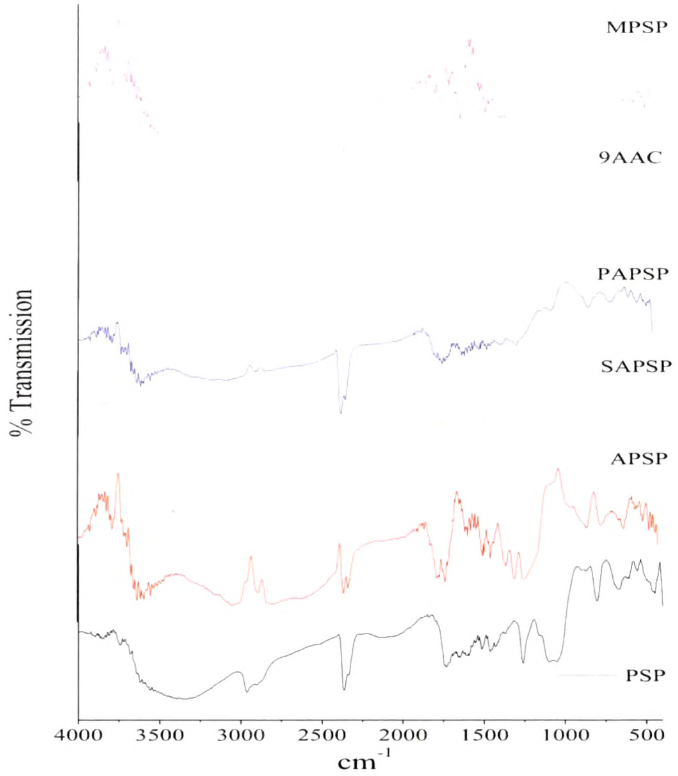

Figure 2.10. Functional group analysis using FTIR

Cyclic compounds containing conjugated C=C and C=N may be responsible for the absorption bands observed at 846 to 809 cm^{-1} except for SAPSP [117-119]. Absorption band in the region 666 to 750 cm^{-1} can be assigned to out-of-plane deformation vibrations of C-H groups located at the edges of aromatic planes [117-127, 128]. The changes observed in FTIR spectra of APSP at 300^{0}C, 600^{0}C, 700^{0}C and 900^{0}C are an evidence for the formation of structures containing multiple carbon-carbon bonds as well as the elimination of originally present hydrogen and oxygen atom. The frequencies between 3200 and 3500cm^{-1} may contain stretching of both amine ($-NH_2$) and alcoholic groups (-OH) which disappears on activation to 300^{0}C and higher temperatures suggesting dehydration of cellulosic and ligneous components. Lignin substances in APSP, SAPSP and PAPSP show strong absorption (1510, 1460 and 1379 cm^{-1}) till a temperature of 300^{0}C. As the activation temperature increases from 140 to 300 to 900^{0}C, the peak around 1600cm^{-1} disappears showing the absence of carboxylic acid group as activation temperature increases. A similar phenomenon is seen after acid, persulphate and steam treatment.

The peak intensity of –O–H, –C=O and –C–H becomes weak or disappear with the increase of activation temperature of APSP. The results prove that the structure of activated carbons (6AAC, 7AAC and 9AAC) becomes stable due to the decomposition of functional groups with increasing activation temperature.

2.3.9. X-Ray Photoelectron Spectroscopic Analysis.

The wide scan XPS spectra of adsorbents are presented in Figure 2.11 and the corresponding binding energies with relative content of species studied are listed in Table 2.9.

Table 2.9. Summary of binding energy and area ratios of carbons

Sample Surface	Proposed components	Binding Energy(eV)	FWHM(eV)	Relative Quantity
	C1s Valence State			
PSP	C-(C, H) graphitic C	284.661	2.310	0.6906
	C-(O, N, H) phenolic, alcoholic, etheric	285.984	1.774	0.1871
	C=O, O-C-O, COOR -carbonyl or quinine	287.200	2.495	0.1223
APSP	C-(C, H)	284.647	2.462	0.6716
	C-(OH, OR)	286.599	2.074	0.2112
	O=C-O	288.577	2.605	0.1172
SAPSP	C- (C, H)	284.524	2.264	0.5272
	C-(OH, OR)	286.342	1.894	0.2499
	O=C-O	288.073, 289.791	1.973, 2.181	0.1471, 0.0758
PAPSP	C-(C, H)	284.590	2.051	0.6297
	C-(OH, OR)	286.071	2.204	0.2552
	C=O, O-C-O, COOR	287.979	1.527	0.0817
	O=C-O	289.308	1.424	0.0334
9AAC	C-(C, H)	284.507	2.336	0.5552
	C-(OH, OR)	286.511	2.284	0.2822
	C=O, O-C-O, COOR	288.384	2.572	0.1155
	C=C, occluded CO, π electrons in aromatic ring, CO_2	290.295	3.464	0.0471
MPSP	C-(C, H, R), C-(C, H)	284.624	2.460	0.5456
	C-(OH, OR)	286.116, 286.346	1.718, 2.120	0.2137, 0.1311
	C=O, O-C-O, COOR O=C-O	288.517	2.491	0.1095

O1s Valence State				
PSP	C=O, C-O (Lactones, phenolic and etheric)	531.400	2.050	0.4424
	Singly bonded oxygen C-O	532.846	2.072	0.5576
APSP	C=O, C-O (Lactones, phenolic and etheric)	531.770	2.606	0.8160
	Singly bonded oxygen C-O	533.570	2.394	0.4796
SAPSP	C=O (Carboxylic acid)	532.209, 534.596	3.492, 3.517	0.8032, 0.1968
PAPSP	C=O, C-O (Carboxylic acid, etheric, lactonic, anhydrides, pyrones and phenols)	531.656 533.388	2.449 3.347	0.4576 0.5424
9AAC	C=O, C-O (Carboxylic acid, etheric, lactonic, anhydrides, pyrones and phenols)	533.080	3.389	0.8437
	Occluded CO, chemisorbed CO_2, O_2 and H_2O	535.638	3.618	0.1563
MPSP	C=O, C-O (Carboxylic acid, etheric, lactonic, anhydrides, pyrones and phenols)	531.367 532.931	2.440 2.978	0.3795 0.6205
N1S				
PSP	C-N-C (pyrrolic nitrogen, pyridines)	399.839, 398.597, 400.846	1.492, 1.512, 1.258	0.6129, 0.2141, 0.1729
APSP	C-N-C (pyrrolic nitrogen, pyridones)	399.98, 400.075	1.228, 1.468	0.3556, 0.2780
	Quartenary nitrogen, protonated pyridinic ammonium ions, nitrogen atoms replacing carbon in graphene	401.278	1.908	0.3664
SAPSP	C-N-C (pyrrolic nitrogen, pyridones)	399.797	1.366	0.3883
	Quartenary nitrogen, protonated pyridinic ammonium ions, nitrogen atoms replacing carbon in graphene	401.477	1.941	0.6118
PAPSP	C-N-C (pyrrolic nitrogen, pyridones)	398.584, 399.774	1.097, 1.319	0.2677, 0.4869
	Quartenary nitrogen, protonated pyridinic ammonium ions, nitrogen atoms replacing carbon in graphene	401.074	1.032	0.2454
9AAC	C-N-C (pyrrolic nitrogen, pyridones)	397.686, 400.803	1.516, 1.596	0.3000, 0.3745
	Oxidised nitrogen functionalities or NO_2 groups	402.300	1.639	0.3255
MPSP	C-N-C (pyrrolic nitrogen, pyridones)	398.703, 400.000	1.889, 1.679	0.2787, 0.5613
	Quartenary nitrogen, protonated pyridinic ammonium ions, nitrogen atoms replacing carbon in graphene	401.606	1.570	0.1599

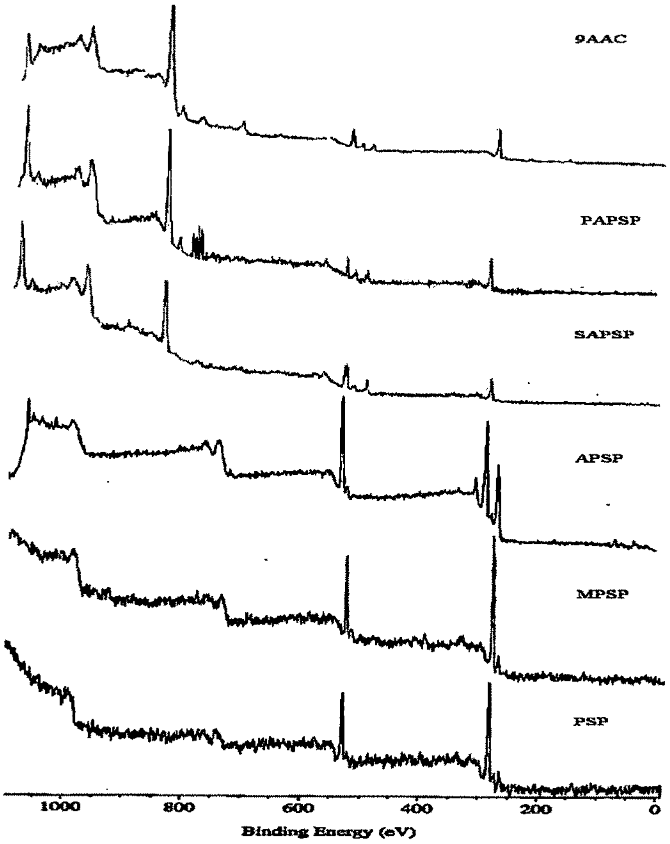

Figure 2.11. Wide scan XPS spectra of adsorbents

Cls spectra (Figure 2.12) can be deconvoluted into six components corresponding to graphitic carbon in PSP, MPSP, APSP, SAPSP, PAPSP, 9AAC (peak 1, ~284.6 eV), aliphatic or defect carbon in PSP (peak 2, ~285.1 eV), carbon in single C-O bonds as ether, alcohol, phenol in MPSP, APSP, SAPSP, PAPSP, 9AAC (peak 3, ~286.6 eV), carbon in carbonyl groups of PSP, MPSP, SAPSP, PAPSP, 9AAC (peak4,~ 287.5 eV), carbon in carboxyl or ester groups of MPSP, APSP, SAPSP, PAPSP (peak 5, ~289.3 eV) and the π-π^* shake-up peak in 9AAC (peak 6, 290.6 eV). Comparison of XPS spectra with those of pure lignin and pure cellulose coupled with pyrolysis studies [127-129] have previously shown that the relatively high content of peak 1 can be attributed to the presence of fatty acid.

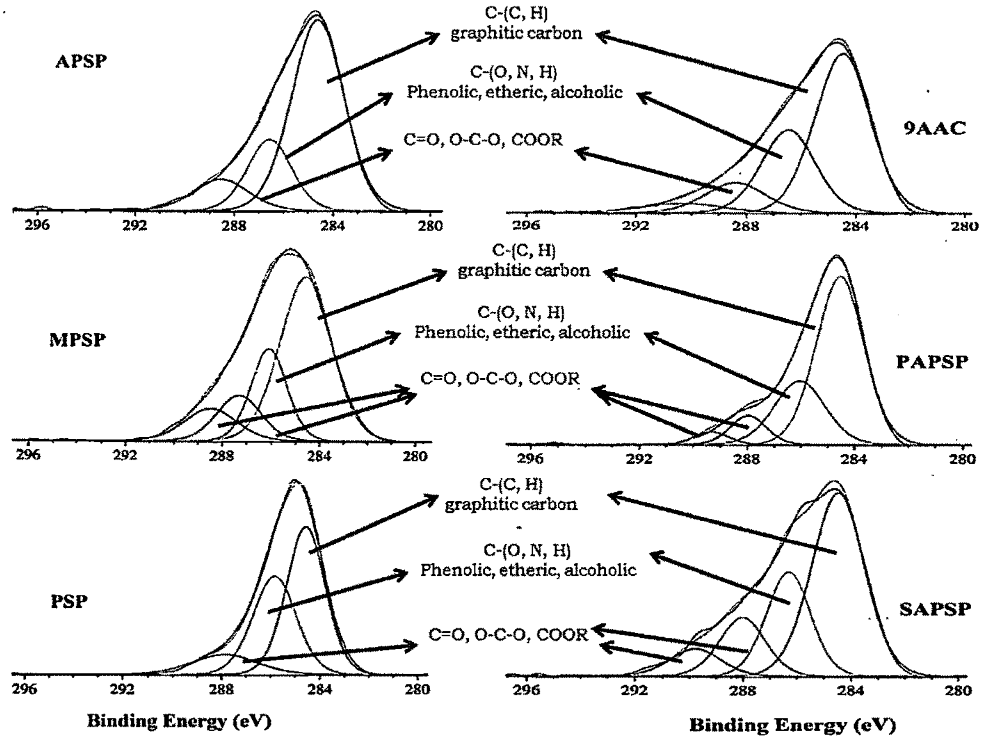

Figure 2.12. C1s XPS deconvolution spectra of adsorbents

The O1S peaks indicate two different chemical states of oxygen (Figure 2.13). The C=O and carboxyl increased for APSP, SAPSP, PAPSP, 9AAC and MPSP as compared to PSP with the maximum increase being observed for 9AAC and SAPSP. This suggested that a more stable structure was formed after modification. Peak I (531.3–531.6 eV) corresponds to C=O groups (ketone, lactone, carbonyl) MPSP, APSP, peak II (532.2– 533.0 eV) to carbonyl oxygen atoms in esters, amides, carboxylic anhydrides which is consistent with the carbon being acidic in nature and oxygen atoms in hydroxyls or ethers PSP, MPSP, SAPSP and peak III (533.9–534.5 eV) to the oxygen atoms in carboxyl groups SAPSP [130-138]. The peak for 9AAC at BE = 535.6 eV is ascribed to chemisorbed oxygen and water [130, 139].

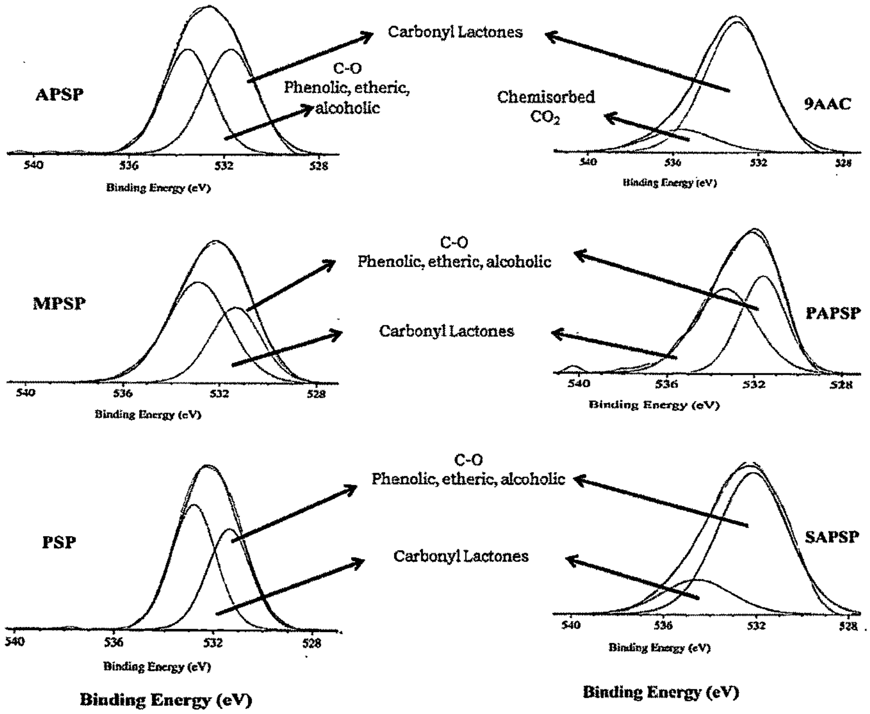

Figure 13. O1s XPS deconvolution spectra of adsorbents

The analysis of N 1S peaks for PSP, MPSP, APSP, SAPSP, PAPSP, 9AAC reveals two peaks at 400.4 and 401.0 eV which can be regarded as characteristic of pyrrolic nitrogen, pyrridones, or a mixture of both. After modification with sulphuric acid the peak becomes characteristic of quaternary nitrogen or protonated pyridinic ammonium ion [140]. It was observed (Table 2.10) that PSP found possess the highest amount of phenolic or etheric group. Acid treatment leads to decreased number of phenolic groups but increased graphitic content than PSP. Further treatment with steam, persulphate and heat resulted in increased amount of oxygen containing groups which resulted due to oxidation of cellulosic ether linkages and aldehydic groups to hemicelluloses and carboxylic acid groups. The O/C ratios are seen to be in the order SAPSP~PAPSP~APSP<MPSP<PSP<9AAC.

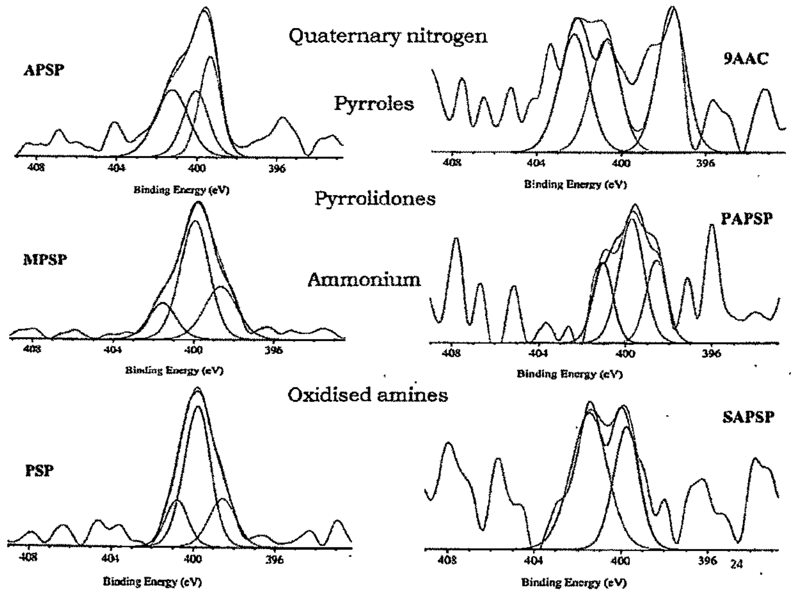

Figure 2.14. N1s XPS deconvolution spectra of adsorbents

Table 2.10. Surface concentration of C, N, O in the adsorbents

Samples	**Cox/Cg**	**Surface concentration (from C 1s peak)%**				
Native		C in graphite	Phenol-ether	Carbonyl-quinone	Carboxyl	Others
PSP	0.951	51.20	37.40	11.41	-	-
APSP	0.489	67.16	21.12	-	11.72	-
SAPSP	0.896	52.72	24.99	14.71	7.58	-
PAPSP	0.587	62.97	25.52	8.17	3.34	-
9AAC	0.801	55.52	28.22	-	11.55	4.71
MPSP	0.832	54.56	21.37	13.11	10.95	-
Native	**XPS (C, N, O)**			**O/ C ratio**		
PSP	58.00, 2.16, 39.84			0.687		
APSP	49.16, 1.17, 49.67			1.011		
SAPSP	43.79, 0.55, 55.66			1.273		
PAPSP	45.01, 0.65, 54.34			1.201		
9AAC	61.57, 0.68, 37.76			0.612		
MPSP	53.03, 1.94, 45.04			0.849		

2.3.10. Solid state-NMR Spectroscopic Analysis.

^{13}C solid state NMR spectra of free and metal loaded adsorbents was done and presented in Figure 2.15, the peaks assigned to different carbons are shown in Table 2.11.

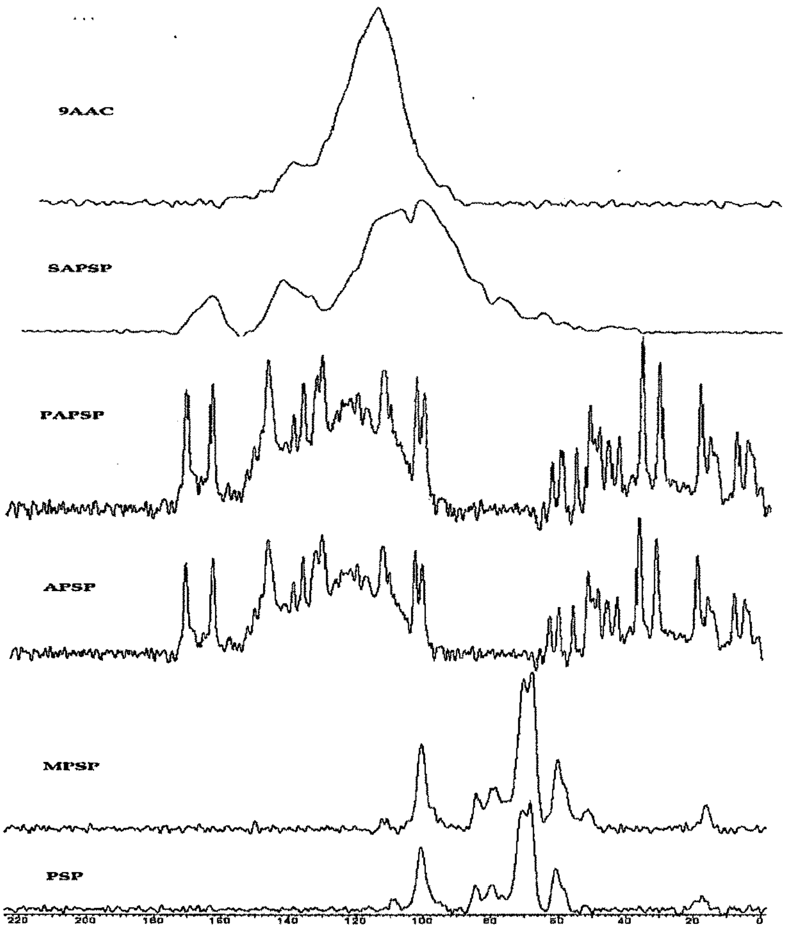

Figure 2.15. Solid state ^{13}C NMR of adsorbents

Relatively sharp signals are assigned to ordered cellulose or hemicelluloses, while broader background signals are assigned to lignin and disordered hemicelluloses [143]. For lignin, we can identify the resonance lines near 50-55 ppm associated with methoxyl groups in PSP, APSP, SAPSP, PAPSP and MPSP [135] and between 115 and 150 ppm for aromatic carbons [141, 142]; the resonance lines due to aliphatic side chains in lignin are concealed by the stronger cellulose and hemicellulose peaks. The bands due to aliphatic carbon show weak resonance in PSP and MPSP and are absent in SAPSP and 9AAC. However these bands are more pronounced in APSP and PAPSP. In particular, the peaks around 17 ppm and 172 ppm in APSP, SAPSP and PAPSP can be attributed to methyl C and carbonyl C in acetyl groups of hemicelluloses, respectively [139].

Table 2.11. Assignments to the NMR peaks

PSP	APSP	SAPSP	PAPSP	9AAC	MPSP	Range	Assignment
-	171	**170**	171	-		195-165	RCOO-RH (Standard oxidized cellulose) Carboxyl carbon of acetate group of hemicelluloses
-	164	-	163/146	-		169-140	C_6H_5O-RH Phenolic carbon
-	-	**147**	-	-		150-140	Subsituted oxygenated aromatic carbon
-	130	-	130	123		135-120	Non oxygenated Aromatic carbons, Aromatic acids and anhydrides
100	101	**111**	101	-	112, 101	102-108	Anomeric carbon (Anhydroglucose) C1
82	-	-	-	-	84, 79	81-93	Anomeric carbon (Anhydroglucose) C4 amorphous cellulose~84
60, 70	62	-	61, 55	-	72, 61, 52	50-70	1^0 Alcohol of (Anhydroglucose) Aliphatic C-O C2, C3, C5(~70) C6 (~60) amorphous cellulose ~62
17	48, 36, 30, 18, 6	-	48, 35, 31, 16, 6	-	17	5-50	Aliphatic C-C possibly of polymethylene type

The signals located at 82-85 ppm in PSP and MPSP can be attributed to C-4 in amorphous cellulose. The peaks between 71 ppm and 74 ppm in PSP and MPSP can be assigned to C-2, C-3, and C-5 in cellulose, whereas the strong peak at 102-110 ppm in PSP, APSP, SAPSP, PAPSP and MPSP can be attributed to anomeric carbon (C-1). The peaks in the region of 130–138 ppm were assigned to the ring carbons in which the ring was not substituted by strong electron donors such as oxygen and nitrogen [142]. The multiple peaks in the range of 147 ppm in SAPSP and PAPSP are due to the carbons of phenolic components, mainly the syringyl and guaiacyl units in lignin. The peak at 146 ppm can be attributed to C-4 in guaiacyl unit with free phenolic OH at C-4 [143] whose signal is strong in SAPSP and moderately strong in PAPSP [139, 144].

When thermal treatment at 900°C is applied, the corresponding spectrum (Figure 2.15) shows a single main peak at 123 ppm with a clear loss of all aliphatic and carbonyl groups. This behaviour is rather typical for a strong aromatization/pseudo-graphitization of the material. 9AAC shows (Figure 2.15) bands from carbonyl or carboxyl carbon (190 ppm), sp^2-hybridized carbon in condensed aromatic rings in all carbons (125–143 ppm), alcohol carbon in all carbons except for 9AAC (C-O, 55–70 ppm)and aliphatic carbon in all carbons except for 9AAC (9–44 ppm). Aromatic carbon dominates the spectra for all adsorbents indicating that carbons are composed of condensed aromatic ring system. Overall, the NMR results demonstrate that while lignocellulosic structure is retained in PSP, APSP, MPSP, SAPSP and PAPSP, on the other hand 9AAC has a highly aromatic structure [145]. The changes incurred on the surface of the palm shell powder due to the various treatments are summarized in scheme 2.3.

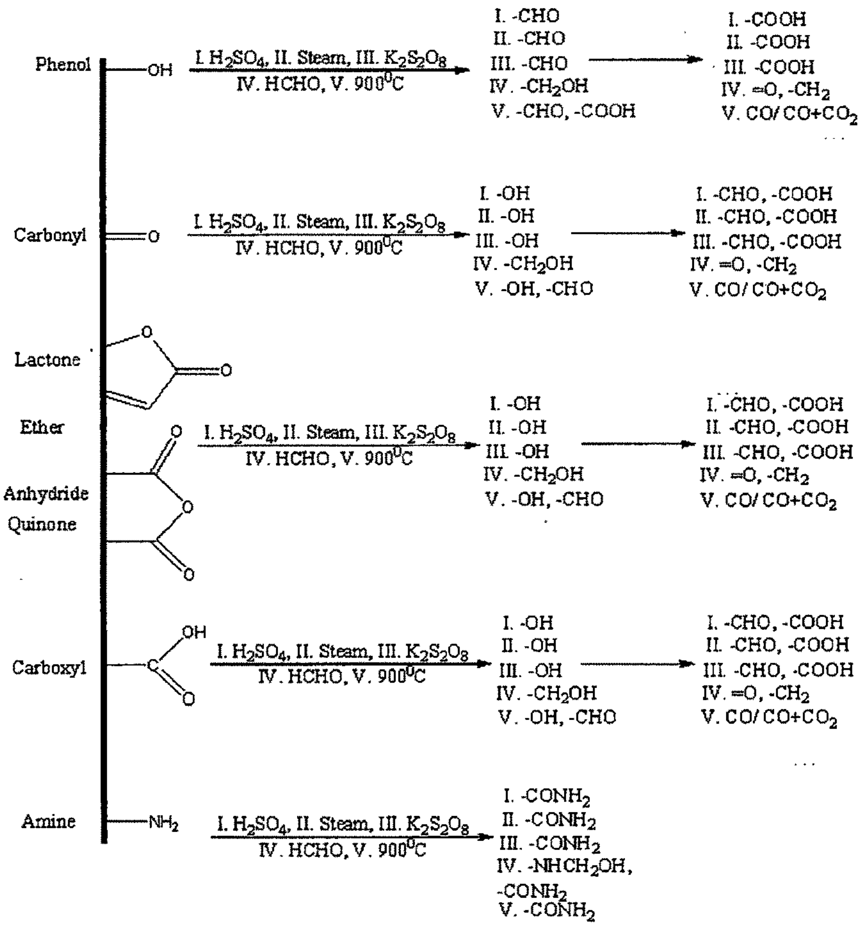

Scheme 2.3. Functional groups of virgin palm shell powder and on modification

2.4. CONCLUSIONS

A series of adsorbents were prepared (PSP, ASPS, SAPSP, PAPSP, MPSP and 9AAC) by giving mild physicochemical treatments as well as thermal activation and their physicochemical properties were compared. Evidence for the change in functional groups produced on treatment of palm shell powder using different physicochemical treatments was provided by FT-IR, XPS and NMR spectroscopic techniques as well as by potentiometric titrations. The prepared adsorbents were also characterized using thermal analysis, X-ray diffraction, nitrogen isotherms and scanning electron microscopic techniques. Potentiometric titrations suggested that all the prepared adsorbents were acidic in nature and also indicated the presence of acid groups with a wide range of pK_a values. All the materials had reasonable iodine values, with 9AAC having an iodine value of about 990 mg/g which is comparable with reported values suggesting reasonable surface areas and micro and mesoporous structures. Though the presence of micro and mesoporous structures were further evidenced by nitrogen isotherms, except for 9AAC, none of the other materials showed good surface areas. This could be probably due to condensation occurring in micropores and capillaries of mesopores which results in underestimation of surface areas. FTIR, XPS and ^{13}CNMR analyses revealed the presence of aldehydic groups along with etheric linkages of lignocellulosic moiety in higher numbers in PSP and MPSP. A small number of amino groups were present in all the adsorbents under study. Furthermore the number of oxygen containing functional groups were also found to increase with acid treatment and oxidation, the order being SAPSP>PAPSP>APSP> MPSP>PSP>9AAC. The prepared materials were found to possess interesting properties. This made us curious to study their adsorption potential for copper, cadmium, zinc, mercury, chromium and uranyl ions, the results of which are shown in chapters 3, 4 and 5.

Literature Cited.

1. O. Ioannidou, A. Zabaniotou. *Renewable and Sustainable Energy Reviews.* **2007**, *11,* 1966.
2. B. Corcho-Corral, M. Olivares-Marin, C. Fernandez-Gonzalez, V. Gomez Serrano, A. Macias Garcia. *Applied Surface Science.* **2006,** *252*, 5961.
3. M. Ahmedna, W.E. Marshall, R.M. Rao. *Bioresour. Technol.* **2000,** *71*, 113.
4. A. Bhatnagar, M. Sillanpaa. *Chemical Engineering Journal.* **2010,** *157*, 277.
5. F.R. Reinoso, M.M. Sabio. *Carbon.* **1992,** *30,* 1111.
6. A.A. El-Hendawy, *Carbon.* **2003,** *41,* 713.
7. R.M. Suzuki, A.D. Andrade, J.C. Sousa, M.C. Rollemberg. *Biores. Technol.* **2007,** *98*, 1985.
8. A.A. El-Hendawy, A.J. Alexander, R.J. Andrews, G. Forrest, *J. Anal. Appl. Pyrolysis.* **2008,** *82,* 272.
9. H.P. Boehm, *Carbon.* **1994,** *32,* 759.
10. J. P. Chen, S. N. Wu, K. H. Chong. *Carbon.* **2003,** *41,* 1979.
11. J. Paul Chen, W. Shunnian. *Langmuir.* **2004,** *20,* 2233.
12. E. Fitzer, K. Mueller, W. Schaefer. The chemistry of the pyrolytic conversion of organic compounds to carbon. In: P. L. Walker (Ed.), Marcel Dekker, New York. *The Chemistry and Physics of Carbon.* **1971,** *7,* 237.
13. Hücknall, D.J. Chemistry of Hydrocarbon Combustion, Ch. 6: Coke and Carbon Formation. *Chapman and Hall, London.* **1985,** 348.
14. I.C. Lewis. *Carbon.* **1982,** *20,* 519.
15. S.J.T. Pollard, G.D. Fowler, C.J. Sollars, R. Perry. *The Science of the Total Environment.* **1992,** *116,* 31.
16. R.F. Rodriguez-Reinoso, A.L. Solano. Microporous structure of activated carbons as revealed by adsorption methods, in: P.A. Thrower (Ed.). *Chemistry and Physics of Carbon,* Marcel Dekker, New York, **1989,** *116.*
17. D. Mohan, C.U. Pittman Jr. *Journal of Hazardous Materials.* **2006,** *B137,* 762.
18. F. Rodriguez-Reinoso, J. Lahaye, P. Ehrburger, Editors. *Fundamental issue in control of carbon gasification reactivity, Netherland, Kluwer Academic* **1991**, 533.
19. K. Tomkow, A. Jankowska, F. Chechowsk, T. Siemieniewska, *Fuel.* **1977,** *56,* 266.
20. C.T. Hsieh, H. Teng, *Carbon.* **2000,** *38,* 863.

21. I. Martin-Gullon, R. Font. *Water Res.* **2001,** *35*, 516.
22. Q. Li, V.L. Snoeyink, B.J. Marinas, C. Campos. *Water Res.* **2003,** *37*, 773.
23. K. Nakagawa, A. Namba, S.R. Mukai, H. Tamon, P. Ariyadejwanich. *Water Res.* **2004,** *37*, 1791.
24. Z. Yue, J. Economy, K. Rajagopalan, G. Bordson, M. Piwoni, L. Ding, V.L. Snoeyink, B.J. Marinas. *J. Mater. Chem.* **2006,** *37*, 3375.
25. S. Han, K. Sohn, T. Hyeon. *Chem. Mater.* **2000,** *37*, 3337.
26. H. Tamai, T. Kakii, Y. Hirota, T. Kumamoto, H. Yasuda, *Chem. Mater.* **1996,** *8*, 454.
27. A. Oya, S. Yoshida, J. Alcaniz-Monge, A. Linares-Solano. *Carbon.* **1995,** *33*, 1085.
28. T. Kyotani, T. Nagai, S. Inoue, A. Tomita, *Chem. Mater.* **1997,** *9*, 609.
29. S. Han, T. Hyeon. *Chem. Commun.* **1999,** *19*, 1955.
30. Z. Li, M. Jaroniec. *J. Am. Chem. Soc.* **2001,** *123*, 9208.
31. L. Lee, S. Yoon, S.M. Oh, C. Shin, T. Hyeon. *Adv. Mater.* **2000,** *123*, 359.
32. M. Smisek, S. Cerny. *Active Carbon: Manufacture, Properties and Applications. Elsevier, London* **1970.**
33. T. Wigmans. *Carbon* **1989,** *27(1)*, 13.
34. R.P. Bansal, J. P. Donner, F. Stoeckli. *Active Carbon. Marcel Dekker, New York* **1988.**
35. J. L. Figueiredo, M. F. R. Pereira, M. M. A. Freitas, J. J. M. Orfao. *Carbon.* **1999,** *37*, 1379.
36. C. A. Toles, S. Rimmer, J. C. Hower. *Carbon.* **1996,** *34*, 1419.
37. C. A. Toles, W. E. Marshall, M. M. Johns. *Carbon.* **1997,** *35*, 1407.
38. B. S. Girgis, M. F. Ishak, *Mater. Lett.* **1999,** *39*, 107.
39. A. Dandekar, R. T. K. Baker, M. A. Vannice. *Carbon.* **1998,** *36*, 1821.
40. V. Gomez-Serrano, M. Acedo-Ramos, A. J. Lopez-Peinado, C. Valenzuela-Calahorro. *Fuel* **1994,** *73*, 387.
41. J. S. Noh, J. A. Scharwz. *Carbon.* **1990,** *28*, 675.
42. V. Gomez-Serrano, M. Acedo-Ramos, A. J. Jopez-Peinado, C. Valenzuela-Calahorrro. *Thermochim. Acta.* **1997,** *291*, 109.
43. M. Mazet, B. Farkhani, M. Bauhu. *Water Res.* **1994,** *28*, 1609.
44. T. Otowa, Y. Nojima, T. Miyazaki. *Carbon.* **1997,** *35 (9)*, 1315.
45. D. R. Preston, G. Bitton, S. R. Farrah. *Appl. Environ. Microb.* **1990,** *56*, 295.
46. R. Gajardo, J. Diezs, J. Jofre, A. Bosch. *J. Virol. Methods.* **1991,** *31*, 345.

47. F. Julien, M. Baudu, M. Mazet. *Water Res.* **1998**, *32*, 3414.
48. F. Rodriguez-Reinoso. Preparation and characterisation of activated carbons. In: Proceedings of the NATO Advanced Study Institute on Carbon and Coal Gasification. *NATO ASI Series E, Martinus Nijhoff Publishers, Netherlands*, **1986**, *105*, 603.
49. H. Marsh, B. Rand. *Carbon.* **1971**, *9*, 47.
50. F. Kapteijn, J.A. Moulijn. Kinetics of catalysed and uncatalysed coal gasification. *In: Proceedings of the NATO Advanced Study Institute on Carbon and Coal Gasification, NATO ASI Series E, Martinus Nijhoff Publishers, Netherlands*, **1986**, *105*, 291.
51. P.L. Walker, Carbon gasification- A ubiquitous reaction of great importance to mankind. *In: Proceedings of the NATO Advanced Study Institute on Carbon and Coal Gasification, NATO ASI Series E, Martinus Nijhoff Publishers, Netherlands*, **1986**, *105*, 3.
52. A. A. Lizzio, H. Jiang, L. R. Radovic. *Carbon.* **1990**, *28(1)* 97.
53. G. De la Puente, J. J. Pis, J. A. Menendez, P. Grange. *J. Anal. Appl. Pyrolysis.* **1997**, *43*, 125.
54. S. Shin, J. Jang, S. H. Yoon, I. Mochida. *Carbon.* **1997**, *35*, 1739.
55. J. Pastor-Villegas, V. Gomez-Serrano, C. J. Duran-Valle, F. J. Higes- Rolando. *J. Anal. Appl. Pyrolysis.* **1999**, *50*, 1.
56. J. A. Menendez, E. M. Menendez, M. J. Iglesias, A. Garcia, J. J. Pis. *Carbon.* **1999**, *37*, 1115.
57. J.S. Mattson, H.B. Mark Jr., *Activated Carbon, Marcel Dekker,NewYork*, 1971.
58. T. Van der Plas. The Texture and the Surface Chemistry of Carbons. *Physical and Chemical Aspects of Adsorbents and Catalysis* (B. G. Linsen, Ed.), Academic Press, London, **1970.**
59. J. S. Mattson, H. B. Mark, Acfivared Carbon: Surface Chemistry and Adsorption from Solufion. *Marcel Dekker, Inc., New York,* **1971.**
60. M.O. Corapcioglu, C.P. Huang. *Water Res.* **1987**, *21*, 1031.
61. V. A. Garten, D. E. Weiss, J. B. Willis. *Au&. J. Chem.* **1957**, *10*, 285.
62. J.R. Perrich. Activated Carbon Adsorption for Wastewater Treatment. *CRC Press*, **1981.**
63. N.R. Bishnoi, M. Bajaj, N. Sharma, A. Gupta. *Biores. Technol.* **2004**, *91*, 305.
64. V.K. Garg, R. Gupta, R. Kumar, R.K. Gupta. *Biores. Technol.* **2004**, *92*, 79.
65. A. Dhaouadi, L. Monser, N. Adhoum. *J. Hazard. Mat.* **2010**, *181*, 692.
66. A. Ozer, H.B. Pirinc. *J. Hazard. Mat.* **2006**, *B137*, 849.
67. Suhas, P.J.M. Carrott, M.M.L. Ribeiro Carrott. *Bioresour. Technol.* **2007**, *98*, 2301.
68. A. Arulanantham, N. Balasubramaniam, T.V. Ramakrishna. *Metal Finishing.* **1989**, *87*, 51.

69. S. J. Park, B. J. Park, S. K. Ryu. *Carbon.* **1999**, *37*, 1223.

70. C. A. Toles, W. E. Marshall, M. M. Johns. *Carbon.* **1999**, *37*, 1207.

71. M. R. Mostafa. *Adsorpt. Sci. Technol.* **1997**, *15*, 551.

72. S. Biniak, M Pakula, G. S. Szymanski, A. Swiatkowski. *Langmuir.* **1999**, *15*, 6117.

73. ASTM, Standard Test Method for Determination of Iodine Number of Activated Carbon. *ASTM Committee on Standards, ASTM: Philadelphia, PA, USA*, **2006,** 4607.

74. A. Aziz, M.S. Ouali, E.H. Elandaloussi. J. Hazard. Mater. **2009**, *163*, 441.

75. P. Galiatsatou, M. Metaxas, V. Kasselouri-Rigopoulou J. Hazard. Mater. **2002**, *B91*, 187.

76. R. Baccar, J. Bouzid, M. Feki, A. Montiel. J. Hazard. Mater. **2009**, *162*, 1522.

77. P.R.F. Campos, M.Sc. Dissertation. *Departamento de Engenharia Quimica, UEM.* **1996**, 1.

78. P. Brassard, J.R. Kramer, P.V. Collins. *Environ. Sci. Technol.* **1990**, *24*, 195-201.

79. S. Brunauer, P. H. Emmett, E. Teller. *J. Am. Chem. Soc.* **1938**, *60*, 309.

80. C. Naizhen, H. Darmstadt, R. Christian. *Energy & Fuels.* **2001**, *15*, 1263.

81. D.K. Chattopadhyay, B. Sreedhar, V.S.N. Kothapalli Raju. *Ind. Eng. Chem. Res.* **2005**, *44*, 1772.

82. V. H. Pan, G. E. Maciel. *Fuel.* **1993**, *72*, 451.

83. K. Kidena, s. Murata, M. Nomura. *Energy fuels.* **1996,** *10*, 672.

84. M. M. Maroo-valer, J. M. Rocha, C. E. Snape. *Fuel.* **1996**, *75*, 1721.

85. J. M. Andresen, Y. Martin, S. R. Moinelo, M. M. Maroto-Valer, C. E. Snape. *Carbon.* **1998**, 36, 1043.

86. H. A. Resing, D. K. C. Hodgeman, J. A.Baker, E. J. Poziomek. *Carbon.* **1985**, *23*, 395.

87. J. C. C. Freitas, T. J. Bonagamba, F. G. Emmerich. *Energy fuels.* **1999**, *11*, 53.

88. H. Eckert, Y. A. Levendis, R. C. Flagan. *J Phys. Chem.* **1988**, *92*, 5011.

89. H. Pan, M. Pruski, B. C. Gemstein, F. Li, J. S. Lanin. *Phys. Rev. B.* **1991**, *44*, 6741.

90. Y. Maniwa, M. Sato, K. Kume, M. E. Kozlov, M. Tokumoto. *Carbon.* **1996**, *34*, 1287.

91. K. Gergova, N. Petrov, V. Minkova, *J. Chem. Technol. Biotechnol.* **1993**, *56*, 77.

92. P.A. Bazuła, A.H. Lu, J.J. Nitz, F. Schuth. *Microporous and Mesoporous Materials.* **2008**, *108*, 266.

93. K. Gergova, N. Petrov, S. Eser. *Carbon.* **1994**, *32*, 693.

94. L. Krisztina, B. Attila, G.N. Lajos, *Carbon.* **2000**, 38, 1965.

95. J.P. Fraissard. Physical adsorption: experiment, theory, and applications, NATO ASI series *Kluwer Academic Publishers* **1996**, 9.

96. F.R. Reinoso, A.L. Solano. Chemistry and Physics of Carbon, *P.A. Thrower, Marcel Dekker, New York*, **1989**, *21*, 1.

97. S.J. Gregg, K.S.W. Singh. Adsorption surface area and porosity. *New York: Academic press* **1982**, 303.

98. T. Ohba, K. Kaneko. *Langmuir.* **2001**, *17*, 3666.

99. M.J. Remy, G. Poncelet. *J. Phys. Chem.* **1995**, *99*, 773.

100. D. Adinata, M.A.W.D. Wan, M.K. Aroua. *Biores. Technol.* **2007**, *98*, 145.

101. S. Ismadji, S.K. Bhatia. *Langmuir.* **2000**, *16*, 9303.

102. S. Ismadji, S.K. Bhatia. *Langmuir.* **2001**, *17*, 1488.

103. P.T. Williams, A.R. Reed. *J. Anal. Appl. Pyroly.* 2003, *70,* 563.

104. F. Stoeckli, A. Guillot, A. M. Slasli, D. Hugi-Cleary. *Carbon.* **2002**, *40*, 211.

105. N.A. Khan, S. Ibrahim, P. Subramaniam. *Malaysian J. Sci.* **2004**, *23*, 43.

106. K. Kadirvelu, M. Kavipriya, C. Karthika, M. Radhika, N. Vennilamani, S. Pattabhi. *Bioresource Technol.* **2003**, *87*, 129.

107. H. Demiral, I. Demiral, F. Tümsek, B. Karabacakoglu. *Chem. Eng. J.* **2008**, *144*, 188.

108. D. Mohan, K.P. Singh, *Wat. Res.* **2002**, *36*, 2304.

109. G. Sreelatha, S. Kushwaha, V.J. Rao, P.P. Sudhakar. *Ind. Eng. Chem. Res.* **2010**, *49*, 8106.

110. M. Koyama, W. Helbert, T. Imai, J. Sugiyama, B. Henrissat. *Proc. Natl. Acad. Sci. U.S.A.* **1997**, *94*, 9091.

111. K. Marco, S.N. Peter, G.J. Mark, K. Markus. *Environ. Sci. Technol.* **2010**, *44*, 1247.

112. Wentao Huang, Hao Zhang, Yaqin Huang, Weikun Wang, Shaochen Wei, *Carbon.* **2011**, *49*, 838.

113. A.K. Kercher, D.C. Nagle, *Carbon.* **2003**, *41*, 15.

114. O. Paris, C. Zollfrank, G.A. Zickler, *Carbon.* **2005**, *43*, 53.

115. T.J. Bandosz, J. Jagiello, C. Contescu, J.A. Schwarz. *Carbon.* **1993**, *31*, 1193.

116. C.M. Castilla, M.V. Lopez-Ramon, F. Carrasco-Marin. *Carbon.* **2000**, *38*, 1995.

117. B.J. Meldrum, C.H. Rochester. *J. Chem. Soc. Faraday Trans.* **1990**, *86*, 1881.

118. B.J. Meldrum, C.H. Rochester, J. Chem. Soc. *Faraday Trans.* **1990**, *86*, 861.

119. G. Socrates. Infrared Characteristic Group Frequencies, 2nd Edn. *John Wiley and Sons,* Chichester **1994**, 50.

120. P.E. Fanning, M.A. Vannice. *Carbon.* **1993,** *31*, 721.

121. B.J. Meldrum, C.H. Rochester. *J. Chem. Soc. Faraday Trans.* **1990,** *86*, 2997.

122. B.J. Meldrum, C.H. Rochester. *J. Chem. Soc. Faraday Trans.* **1990,** *86*, 3647.

123. M. Nakahara, S. Asai, Y. Sanada, T. Ueda. *J. Mater. Sci.*, **1995,** *30*, 5667.

124. M. Nakahara, Y. Sanada. *J. Mater. Sci.* **1995,** 30 4363.

125. J. Zawadzki. Chemistry and Physics of Carbon. Ed. P. A. Thrower. *'Marcel Dekker, New York.* **1989,** *21*, 147.

126. L. Dupont, E. Guillon. *Environ. Sci. Technol.* **2003,** *37*, 235.

127. S. Biniak, G. Szymanski, J. Siedlewski, A. Swiatkowski. *Carbon.* **1997,** *35*, 1799.

128. A. Gauthier, S. Derenne, L. Dupont, E. Guillon, C. Largeau, J. Dumonceau, M. Aplincourt. *Anal. Bioanal. Chem.* **2002,** *373*, 830.

129. H. Darmstadt, C. Roy. *Carbon.* **2003,** *41*, 2653.

130. H. Chen, A. Wang. *J. Hazard. Mater.* **2009,** *165*, 223.

131. S. Qaiser, A. R. Saleemi, M. Umar. *J. Hazard. Mater.* **2009,** *166*, 998.

132. G. Gilardi, L. Abis, A. E. G. Cass. *Enzyme Microb. Technol.* **1995,** *17*, 286.

133. K. Laszlo, E. Tombacz, K. Josepovits. *Carbon.* **2001,** *39*, 1217.

134. K. K. Pandey. *J. Appl. Polym. Sci.* **1999,** *71*, 1969.

135. W. L. Earl, D. L. VanderHart. *J. Am. Chem. Soc.* **1980,** *102*, 3251.

136. P. T. Larsson, K. Wickholm, T. Iversen. *Carbohydrate Res.* **1997,** *302*, 19.

137. L. Huang, T. Boving, B. S. Xing. *Environ. Sci. Technol.* **2006,** *40*, 3279.

138. C. M. Popescu, P. T. Larsson, C. Vasile. *Carbohyd. Polym.* **2011,** *83*, 808.

139. J. C. C. Freitas, T. J. Bonagamba, F. G. Emmericha. *Carbon.* **2001,** *39*, 535.

140. W. S. Wan Ngah, M. A. K. M. Hanafiah. *J. Environ. Sci.* **2008,** *20*, 1168.

141. A. E. Ofomaja, E. B. Naidoo, S. J. Modise. *J. Hazard. Mater.* **2009,** *168*, 909.

142. V. K. Gupta, A. Rastogi. *J. Hazard. Mater.* **2008,** *152*, 407.

143. L. Huang, Z. Ou, T. B. Boving, J. Tyson, B. Xing. *Chemosphere.* **2009,** *76*, 1056.

144. K. Srividya, K. Mohanty. *Chem. Eng. J.* **2009,** 155, 666.

145. M. Schnitzer, C. M. Preston. *Plant Soil.* **1983,** *75*, 201.